[AMERICAN JOURNAL OF SCIENCE, VOL. 293, MAY, 1993, P. 361–404]

American Journal of Science

MAY 1993

FLUID FLOW AND CHEMICAL REACTION KINETICS IN METAMORPHIC SYSTEMS

ANTONIO C. LASAGA and DANNY M. RYE
Department of Geology and Geophysics, Yale University,
New Haven, Connecticut 06511

ABSTRACT. The treatment and effects of chemical reaction kinetics during metamorphism are developed along with the incorporation of fluid flow, diffusion, and thermal evolution. The interplay of fluid flow and surface reaction rates, the distinction between steady state and equilibrium, and the possible overstepping of metamorphic reactions are discussed using a simple analytic model. This model serves as an introduction to the second part of the paper, which develops a reaction model that solves the coupled temperature-fluid flow-chemical composition differential equations relevant to metamorphic processes. Consideration of stable isotopic evidence requires that we consider such a kinetic model for the chemical evolution of a metamorphic aureole. A general numerical scheme is discussed to handle the solution of the model. The results of this kinetic model allow us to reach several important conclusions regarding the factors controlling the chemical evolution of mineral assemblages during a metamorphic event.

INTRODUCTION

The role of fluids in determining the physical and chemical characteristics as well as the evolution of both the crust and upper mantle has been brought to center stage in recent years. Numerous approaches have been developed that involve analysis of fluid inclusions, changes in mineral assemblages, isotopic signatures, and deformation histories, among others. Some of these approaches have made extensive use of the thermodynamic theory and the thermodynamic experimental data available for some minerals and for a variety of fluid compositions. However, because the chemical properties of the rocks and the fluids in mutual contact have to be determined by the coupling of the fluid transport and the kinetics of heterogeneous chemical reactions, it is imperative that some of the salient features of such a coupling be analyzed and discussed in relation to our current models of fluid-rock interaction. This paper will address several fundamental concepts the authors feel have not been adequately treated in previous petrologic papers.

The paper may be summarized in the following way. In general, because many laboratory experiments reach equilibrium relatively fast, metamorphic rocks and fluids have been modeled assuming essentially instantaneous local equilibrium between rocks and fluids. If this assumption is valid, then the large body of thermodynamic data available can be

used with little modification to model water/rock ratios or estimate metasomatic mass fluxes. A major flaw in such models is that the time required to achieve equilibrium in a laboratory experiment is not the only relevant parameter in models of open system petrologic processes. Rather, from an open process point of view, the important concerns are (A) whether a kinetic steady state is at all possible, given the geological boundary conditions, (B) if a steady state is possible, how long it will take the system to achieve steady state, and (C) having achieved a steady state, how much of the system is in a "permanent" far from equilibrium condition?

It is clear that, at the outset, a clear definition of steady state and its role in petrologic processes must be given. In the petrologic system comprising a set of reacting minerals and a coexisting fluid, the time constants for the variation of the fluid composition will be much shorter than the time required to change significantly the abundance of any one reacting mineral. In this case, the composition of the fluid can be treated as the concentration of a reactive intermediate in the classical kinetic sense (Lasaga, 1981). At any particular position in space, many rates may affect the local composition of the fluid including advection, diffusion, dispersion, and reactions with the surfaces of all minerals present. The behavior of a reactive intermediate is such that in a "short" time its concentration achieves a steady state balance between all the production and all the consumption rates. In the same manner, the composition of the fluid will, in many cases, achieve a steady state (mathematically $\partial c_i/\partial t = 0$ for all components, i, in the fluid), which, for each chemical component, balances the input and the output from all the various processes discussed above.

Steady state will be achieved if the "short" time needed to balance the input and output from all the various processes involved is less than the time variation of any outside process. If a steady state composition is reached it may **not** be and in general will not be the same as the equilibrium composition. The equilibrium composition is reached as a special case of steady state where for each mineral present in the system the input rate to the fluid from the reacting mineral surface is balanced by an equal output rate from the fluid to the mineral surface. For closed systems, equilibrium may be reached, given sufficient time (for example, see fig. 1A). On the other hand, for open systems (fig. 1B) the flux of material in and out of any rock volume element will prevent the system from achieving equilibrium. Instead, a steady state may be reached, and the system will be maintained out of equilibrium for geologically long times. In cases where the outside process varies rapidly, steady state may never be achieved. For example, if one experimentally increases the temperature of a system at a fast pace, the system may never reach a steady state. Non-equilibrium steady states are very common in kinetics and as shall be shown in this paper can play a considerable role in petrologic processes.

Metasomatism results generally from the dissolution, transport, and precipitation of chemical components during the flow of fluids through a

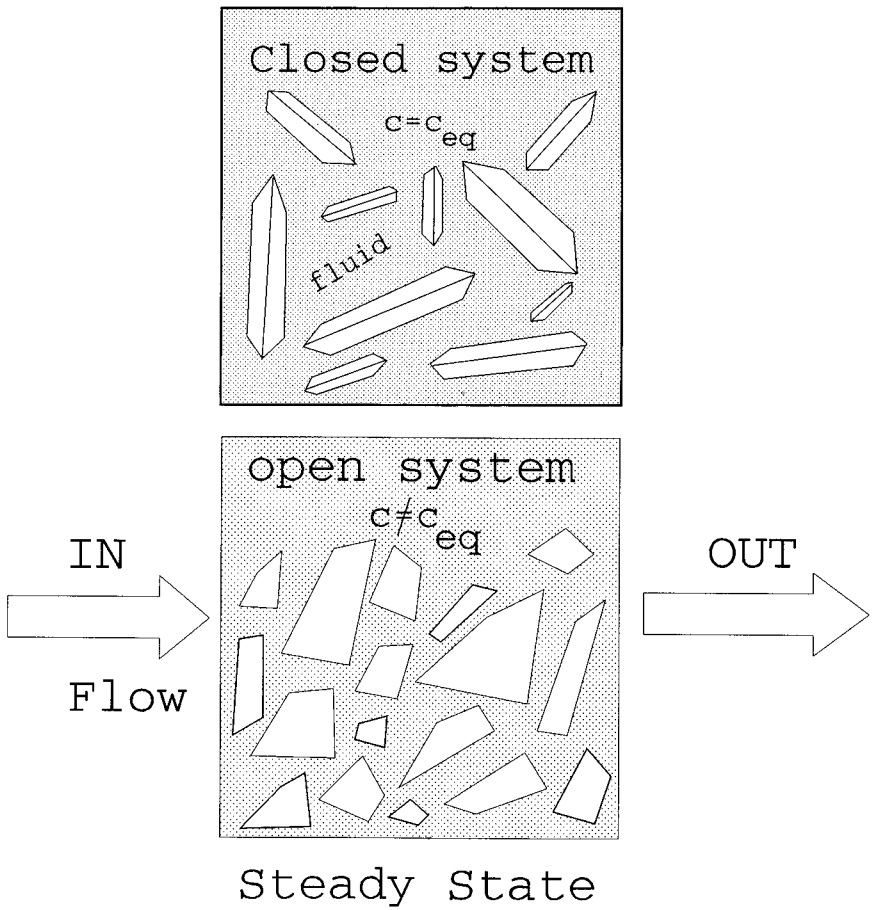

Fig. 1(A) Fluid reacting with mineral assemblage in a closed system. The fluid will eventually reach equilibrium with each mineral. (B) Mineral assemblage reacting with fluid in an open system. The fluid will approach a non-equilibrium steady state.

series of rock units. The understanding of metasomatism, accordingly, must be based on knowing the transport properties of the fluid, for example diffusion/dispersion and/or convective flow, as well as the complex heterogeneous kinetics taking place at every mineral surface in contact with the fluid. Much of the early work on the theory of metasomatism focused on diffusive transport models, which were the most amenable to a thermodynamic treatment because of the assumption of *local equilibrium* (Korzhinski, 1959; Thompson, 1959). These studies did not consider fluid flow, nor did they consider the kinetics taking place at mineral surfaces in contact with the fluid.

In recent years, research has begun to tackle the other three aspects of the problem: fluid flow (Bickle and McKenzie, 1987; Chamberlain and

Rumble, 1988; Connolly and Thompson, 1989; Crawford and Hollister, 1986; Ferry, 1986, 1987; Helgeson and Lichtner, 1987; Lasaga, 1984; Lichtner, 1985, 1988; Rumble and others, 1982; Steefel and Lasaga, 1990; Wood and Walther, 1986; Baumgartner and Ferry, 1991) dispersion (Steefel and Lasaga, 1992), and the rates of surface reactions (Dachs and Metz, 1988; Heinrich, Metz, and Bayh, 1986; Heinrich, Metz, and Gottschalk, 1989; Lasaga, 1986; Schramke, Kerrick, and Lasaga, 1987). This paper will combine these three processes and explore some of the implications for the normal *"modus operandi"* of petrologists in interpretation of field data.

BASIC EQUATIONS

The three differential equations that must be solved in a full treatment of metamorphic reactions are the differential equations governing the temperature, T, the fluid composition, and the fluid flow rate, v. In the case of heat producing (or consuming) chemical reactions and of fluid flow, v (*in m/yr*), the equation governing the change in temperature in one spatial direction, x, is given by:

$$\frac{\partial T}{\partial t} = \kappa \frac{\partial^2 T}{\partial x^2} - \frac{\partial(\gamma v T)}{\partial x} + A(x) \tag{1}$$

where κ is the thermal diffusivity (m^2/yr), v is the *true* velocity of the fluid (m/yr), and the factor γ is given by

$$\gamma = (\rho_{fluid}/\rho_{rock})\,(C_{P,fluid}/C_{P,rock})\phi \tag{2}$$

where ρ is density (g/cm^3), C_P is the specific heat capacity ($cal/g/K$), and ϕ is the porosity of the rock. γ corrects for the difference in density and heat capacity between fluid and rock and for the porosity of the rock. This can be seen by calculating the convective heat flow which is

$$J_{conv} = \phi \rho_{fluid} v C_{P,fluid} T. \tag{3}$$

Division of both sides of the energy continuity equation by $\rho_{rock}C_{P,rock}$ to yield eq (1) will also lead to the γ coefficient. Fluid flow may affect the thermal profile in nature (Bickle and McKenzie, 1987; Brady, 1988; Chamberlain and Rumble, 1988). The velocity field in this study is taken as constant (although the size will vary). Other studies solve for the variation of the flow rate with space and time by use of Darcy's equation along with the other terms discussed here (for example, Cathles, 1977; Steefel and Lasaga, 1990).

Ignoring contributions from radioactive decay, the $A(x)$ term stands for the local heat production due to chemical reactions and is given by

$$A(x) = \sum_j \frac{\Delta H_j R_j \phi}{\rho_{rock} C_{P,rock}} \tag{4}$$

The summation in eq (4) is over all the chemical reactions taking place, and ΔH_j, R_j are the enthalpy (*cal/mole*) and the reaction rate (*moles/cm³ fluid/yr*) of reaction j, respectively.

Although fluid compositions may vary a great deal, for most metamorphic systems, the fluid composition is assumed to be dominantly H_2O and CO_2. The concentrations of these species, c_i (*in moles/cm³ fluid*), are governed by the following equations:

$$\frac{\partial(\phi C_{H_2O})}{\partial t} = \frac{\partial\left(\phi D_{H_2O}\left(\frac{\partial C_{H_2O}}{\partial x}\right)\right)}{\partial x} - \frac{\partial(\phi v c_{H_2O})}{\partial x} + R_{H_2O}\phi \tag{5}$$

$$\frac{\partial(\phi C_{CO_2})}{\partial t} = \frac{\partial\left(\phi D_{CO_2}\left(\frac{\partial C_{CO_2}}{\partial x}\right)\right)}{\partial x} - \frac{\partial(\phi v c_{CO_2})}{\partial x} + R_{CO_2}\phi \tag{6}$$

The D's refer to the combined molecular diffusion (including tortuosity effects) and dispersion coefficient in the fluid (m^2/yr), and R is the net production rate of H_2O or CO_2 from all local chemical reactions in units of *moles/cm³ fluid/yr*.

The kinetic modeling requires that the composition of the fluid expressed, as the mole fraction of CO_2, X_{CO_2}, be converted to concentration, c_{H_2O} and c_{CO_2}, in units of *moles/cm³ fluid*. In general, we have the exact relation:

$$c_{H_2O} = \frac{X_{H_2O}}{\overline{V}} \tag{7}$$

$$c_{CO_2} = \frac{X_{CO_2}}{\overline{V}} \tag{8}$$

where $\overline{V}$ is the molar volume of the fluid. $\overline{V}$ can be obtained from a modified Redlich-Kwong equation of state or other similar equations of state:

$$\left(P + \frac{a}{(\overline{V}^2 + b\overline{V})\sqrt{T}}\right)(\overline{V} - b) = RT \tag{9}$$

where $\overline{V}$ is the molar volume, and a, b depend on temperature and the composition of the fluid (Kerrick and Jacobs, 1981).

In this paper, ϕ, v, D are treated as constants to simplify the understanding of the results and to establish the importance of the kinetic concepts introduced. Future papers will deal with both two dimensional and fully coupled hydrologic-chemical-thermal equations as in Steefel and Lasaga (1990). If ϕ, v, D are constants then the dynamic equations reduce to:

$$\frac{\partial C_{H_2O}}{\partial t} = D_{H_2O}\frac{\partial^2 C_{H_2O}}{\partial x^2} - v\frac{\partial C_{H_2O}}{\partial x} + R_{H_2O} \tag{10}$$

$$\frac{\partial C_{CO_2}}{\partial t} = D_{CO_2} \frac{\partial^2 C_{CO_2}}{\partial x^2} - v \frac{\partial C_{CO_2}}{\partial x} + R_{CO_2} \tag{11}$$

The next section considers some simple models that elucidate the significance of the coupling of the transport terms to the reaction terms, R_{H_2O}, and R_{CO_2}, in eqs (10) and (11).

A simple flow and reaction model.—The chemical differences between open and closed systems are major. These differences have been stressed in Lichtner (1985, 1988), Lassey and Blattner (1988), Ague and Brimhall (1989), Steefel and Lasaga (1990), and Lasaga (1989). An important illustration of the fundamental differences is immediately derived from consideration of the kinetic equation for the concentration, c, of a component in a moving fluid. If there is little diffusion and dispersion, constant porosity and constant fluid flow rate, v, then c obeys the equation,

$$\frac{\partial c}{\partial t} = -v \frac{\partial c}{\partial x} + R_{chem} \tag{12}$$

where the constant direction of flow has been taken as the x-axis, and where R_{chem} (*in moles/cm*^{3} *fluid/yr*) refers to the sum of all the chemical reactions involving the component. Normally a fluid would percolate and enter a region of active chemical reaction. For example, a fluid undersaturated with respect to calcite or dolomite could penetrate a region of impure cabonates (fig. 2). Let us label the beginning of the chemically active region $x = 0$. Suppose that the chemical reaction rate is such that a simple **linear** term adequately describes it. Such is the case for the dissolution/precipitation of quartz for which the R_{chem} is given by:

$$R_{chem} = k_{eff}(c_{eq} - c) \tag{13}$$

The label k_{eff} is being used because this rate constant incorporates the effect of a variety of factors such as surface area (see below). Using eq (13)

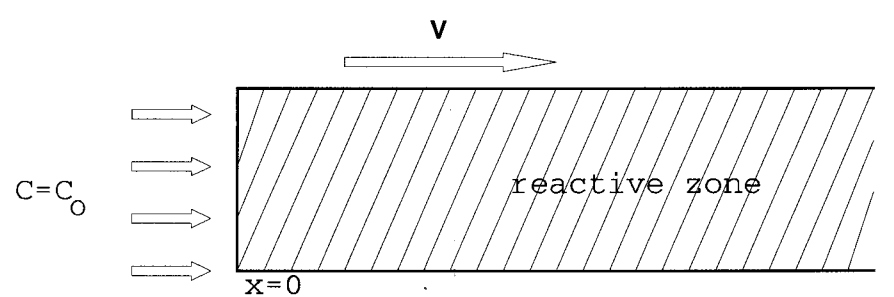

Fig. 2. Sketch of the simple chemical reaction-fluid flow-thermal model. The reaction zone begins at $x = 0$. A non-equilibrium fluid flows from the left at some rate v.

the differential eq (12) becomes

$$\frac{\partial c}{\partial t} = -v\frac{\partial c}{\partial x} + k_{eff}(c_{eq} - c) \tag{14}$$

In eq (14), k_{eff} is the net rate coefficient and has units of $time^{-1}$; c_{eq} is the equilibrium concentration of the chemical species with the solids present (for example $X^{eq}_{CO_2}/\overline{V}_{CO_2}$), and it is taken as uniquely fixed here (for example, no variation in c_{eq} due to temperature changes is considered). Laboratory measurements far from equilibrium (very undersaturated so that $c \sim 0$) provide an overall rate according to eq (13) of $k_{eff}\, c_{eq}$ (*in moles/cm*^{3}*/yr*). This rate can also be obtained from the surface reaction rate constant for dissolution, k_{diss}, discussed in Lasaga (1984). k_{diss} refers to the surface reaction rate, and it has units of *moles/cm*^{2} *mineral surface/yr*. However, the rate R_{chem} in eq (14) requires units of concentration/unit time or *moles/cm*^{3} *fluid/yr*. Therefore, to convert k_{diss} to the appropriate units it is necessary to incorporate the surface area to volume of fluid ratio, that is $R_{chem} = (A/V)\, k_{diss}$, where A/V represents the area of mineral per unit volume of fluid (*cm*^{2} *mineral surface/cm*^{3} *fluid*) (see Lasaga, 1984). As a result, $R_{chem} = k_{eff}\, c_{eq} = (A/V)\, k_{diss}$, and the constant k_{eff} (in yr^{-1}) can be evaluated from,

$$k_{eff} = \frac{A}{V}\frac{k_{diss}}{c_{eq}} \tag{15}$$

Note that if A is the mineral surface area per unit volume of rock then $A/V = A/\phi$, where ϕ is the porosity of the rock. The concentration, c, varies only as a function of time. Eq (14) can be rewritten using the relation

$$\frac{dc}{dt} = \frac{\partial c}{\partial t} + v\frac{\partial c}{\partial x}$$

as

$$\frac{dc}{dt} = k_{eff}(c_{eq} - c)$$

this last equation can be solved for $c(t)$ which, if k_{eff} is constant, has the solution,

$$c(t) = c_{eq} + (c_o - c_{eq})e^{-k_{eff}t} \tag{16}$$

The value of c in the incoming solution at $x = 0$ is taken to be c_o. Because movement is only due to fluid flow, a packet of fluid moves a distance of $x = vt$ in time t, if v is constant. As a result, the last equation, which now represents steady state, can be rewritten replacing t by x/v,

$$c_{st}(x) = c_{eq} + (c_o - c_{eq})\exp\left(-\frac{k_{eff}}{v}x\right) \tag{17}$$

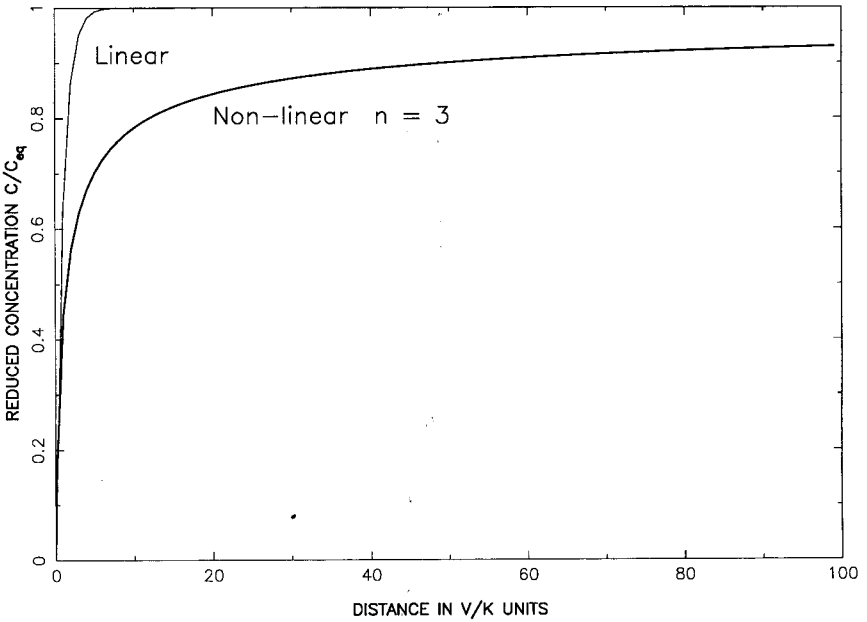

Fig. 3. Steady state curves showing the variation in the concentration ratio c/c_{eq}, as a function of the distance from the beginning of the reaction zone. Distance is given in units of v/k (see text). Both linear and non-linear steady states are given. Note the much slower approach to equilibrium in the non-linear case.

a solution used in many other kinetic analyses. Figure 3 shows the solution concentration as a function of distance; obviously, over long enough distances, the fluid reaches equilibrium with the medium. The minimum distance required for c_{st} to be within 5 percent of equilibrium, that is, for $c_{st}/c_{eq} = 0.95$, is calculated dividing eq (17) by c_{eq} as

$$\left(1 - \frac{c_o}{c_{eq}}\right) \exp\left(-\frac{k_{eff}}{v} x\right) = 0.05$$

If c_o/c_{eq} is rather small so that the term in parentheses is essentially unity then $x_{\min}$ is given by

$$x_{\min} = 3.0 \frac{v}{k_{eff}} \tag{18}$$

Consequently, the ratio v/k_{eff} becomes a *characteristic distance*. Note that this distance is a steady state distance and that the non-equilibrium condition within this distance remains fixed for long times, a point discussed further below.

This characteristic distance can be contrasted with that obtained in the case where the chemical kinetics are **non-linear.** Suppose that the rate law is given by

$$R_{chem} = k'(c_{eq} - c)^n \tag{19}$$

where n is **not** necessarily equal to 1. First, to compare the two rate laws we must assume that far from equilibrium, the mineral governing the reaction dissolves at a given fixed measured rate, that is, the mineral reaction rate that was measured lies in what is termed the "dissolution plateau" (Nagy, Blum, and Lasaga, 1991). We will then make both rate laws conform to this experimental datum. The two rate laws (eqs 13 and 19) should converge on this rate as c approaches 0:

$$R_{chem} = k_{eff} c_{eq} = k' c_{eq}^{n} \tag{20}$$

Using this last equation to eliminate $k'(=k_{eff}/c_{eq}^{n-1})$ in eq (19) and inserting this expression for R_{chem} into eq (12) yields a new non-linear differential equation:

$$\frac{\partial c}{\partial t} = -v \frac{\partial c}{\partial x} + k_{eff} c_{eq} \left(1 - \frac{c}{c_{eq}}\right)^{n} \tag{21}$$

Once more, this equation can be readily solved for c as a function of time. After replacing t by x/v, the result is,

$$c(x) = c_{eq} - c_{eq} \frac{1 - \dfrac{c_o}{c_{eq}}}{\left[1 + (n-1)\left(1 - \dfrac{c_o}{c_{eq}}\right)^{n-1} \dfrac{k_{eff}}{v} x\right]^{\frac{1}{n-1}}} \tag{22}$$

Setting c_o/c_{eq} near zero, the minimum distance required to achieve 95 percent of equilibrium is given by,

$$\left[1 + (n-1) \frac{k_{eff}}{v} x_{min}\right]^{-\frac{1}{n-1}} = 0.05$$

or,

$$x_{\min} = \frac{20^{n-1} - 1}{n - 1} \frac{v}{k_{eff}} \tag{23}$$

Figure 3 illustrates the much flatter approach to equilibrium for the non-linear case. For example, if $n = 3$, then $x_{min} = 200\, v/k_{eff}$. Such large values for x_{min} suggest that non-linear rate laws will produce much more extended regions of non-equilibrium. Non-linear rate laws may be quite prevalent in mineral-fluid reactions (Lasaga, 1986). Table 1 gives the calculation of x_{min} for a variety of values of fractional equilibration and n.

A fundamental result of this section is that no matter how large the kinetic rate constant, k_{eff}, there will always be a region of **constant** deviation from equilibrium within a distance measured not by k_{eff} alone but by the ratio v/k_{eff} and by the non-linearity of the rate law. Note that this region will **never** reach equilibrium. As a result, the mineral reactions

TABLE 1

Equilibrium distances in units of v/k

Percent Equilibrium	n					
	1	2	3	4	5	6
95	3.00	19.0	200	2670	40000	640000
90	2.30	9.0	50	333	2500	20000
80	1.61	4.0	12	41	156	625

will proceed at a non-negligible rate for long times. The only way to change the steady state is to begin to remove reactants completely. As the abundance of a reactant mineral decreases, its area, A, will drop and so will k_{eff} (see eq 15). This is our first introduction into the **kinetic isograd** (Lasaga, 1989).

Within the zone where there is constant and marked deviation from equilibrium, there will be significant extent of reaction. Therefore, in this zone, reactions will take place until one of the reactants is consumed (Lasaga, 1986). As a result, the $x = 0$ boundary will progress into the reaction zone, as a reactant phase is consumed (see fig. 4). This behavior will produce mineral variations across a reaction zone that looks similar to the variation predicted for equilibrium reactions. Such behavior will produce a moving boundary separating reacted from non-reacted regions. This boundary is a "*kinetic isograd.*" The sharpness of the reacting region, or the minimum width separating regions with no reactant present from regions with all the original reactant present, will depend on the kinetics of the overall reactions as well as the rate of temperature variations.

KINETIC MODEL INCLUDING DIFFUSION AND DISPERSION

At this point it is very useful to introduce another simple kinetic model that will aid greatly in framing the non-equilibrium aspects of reacting fluids in metamorphic events. In the simplest linear kinetic case, the change in the concentration of a component in a fluid for a process that allows for fluid flow, diffusion, dispersion, and chemical reaction obeys the equation:

$$\frac{\partial c}{\partial t} = D\frac{\partial^2 c}{\partial x^2} - v\frac{\partial c}{\partial x} - k_{eff}(c - c_{eq}) \tag{24}$$

The composition of the fluid will be fixed at the beginning of reaction (that is, $x = 0$) to some value, c_o. Therefore, we introduce the boundary condition:

$$c(x = 0,t) = c_o \tag{25}$$

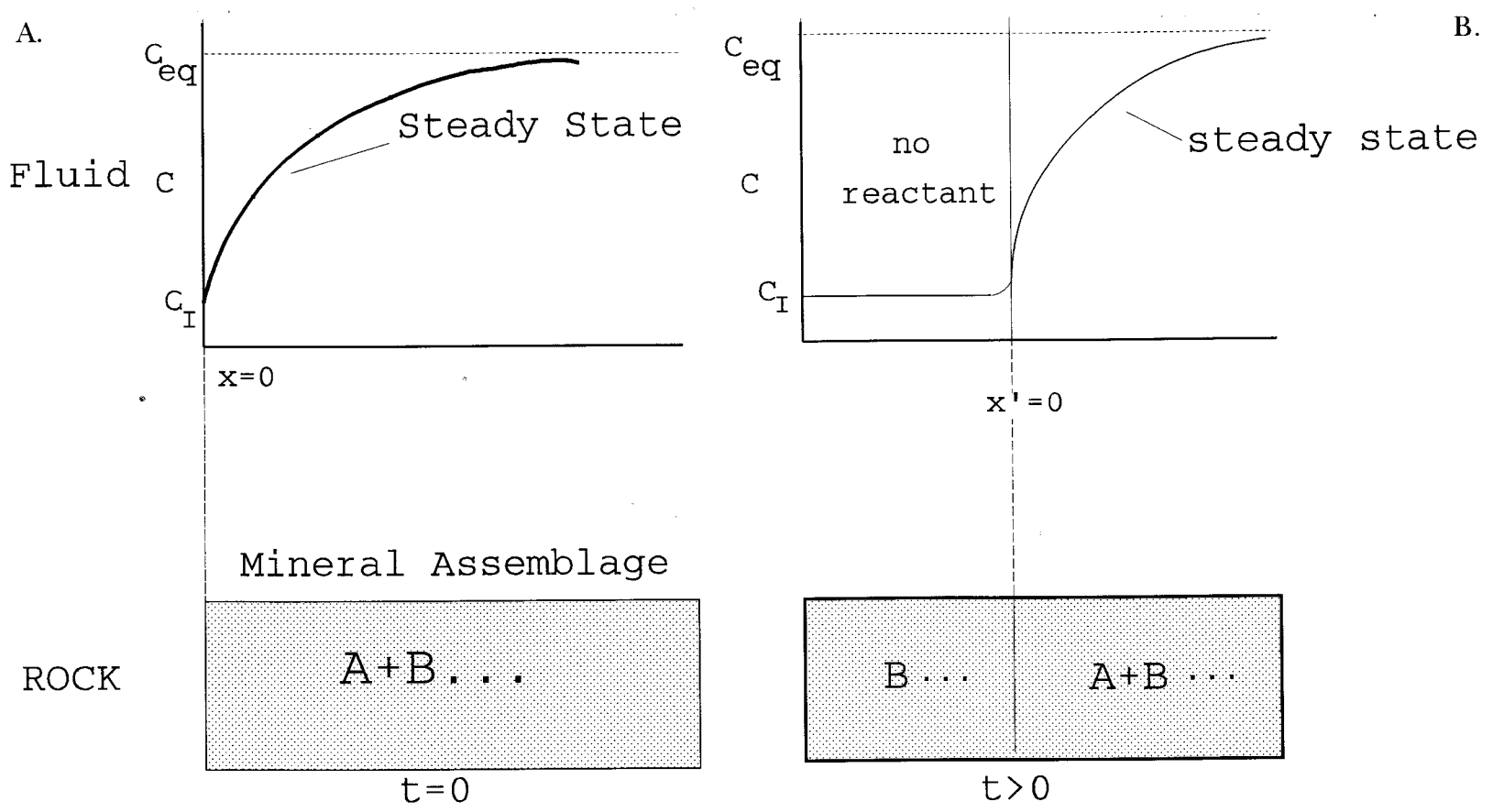

Fig. 4. Sketch illustrating the development of a kinetic isograd. (A) At $t = 0$, the reaction zone contains both minerals A and B (reactants in a given metamorphic reaction). A steady state profile is shown, which maintains the system far from equilibrium close to $x = 0$. Therefore, extensive chemical reaction can take place in the region where $c \neq c_{eq}$ and the amount of minerals A and B will decrease. (B) At some later time, t, all of A has disappeared from the region marked "no reactant" (assuming that there was less A than B). A reaction front has developed, and the reaction now begins to occur at the new position, x'. This moving front will appear as an isograd in the field.

If the initial composition of the fluid in the reaction zone is $g(x)$ (which can simply be the equilibrium composition), then we have the initial condition

$$c(x, t = 0) = g(x) \tag{26}$$

Using the last two equations, eq (24) can be solved by the following solution:

$$c(x, t) = (c_o - c_{eq})e^{-Sx} + c_{eq} + \frac{e^{-\left(k_{eff} + \frac{v^2}{4D}\right)t}}{2\sqrt{\pi D t}} \int_0^\infty [f(x')e^{-\frac{v}{2D}(x'-x)}] \cdot [e^{-(x'-x)^2/4Dt} - e^{-(x'+x)^2/4Dt}]\, dx' \tag{27}$$

where S is given by

$$S = \frac{\sqrt{(v^2 + 4Dk_{eff})}}{2D} - \frac{v}{2D} \tag{28}$$

and

$$f(x) = c(x, 0) - (c_o - c_{eq})e^{-Sx} - c_{eq} \tag{29}$$

After sufficiently long times (that is as $t \to \infty$), the last term in eq (27) disappears, and the concentration reaches a steady state value, $c_{st}(x)$, which varies only with position:

$$c_{st}(x) \equiv (c_o - c_{eq})e^{-Sx} + c_{eq} \tag{30}$$

Note that eq (30) reduces to eq (17) if $D \to 0$.

Generalizations can be made if we rewrite eq (27) in dimensionless form by introducing the following characteristic time, τ, and length, χ:

$$\tau \equiv \left(k_{eff} + \frac{v^2}{4D}\right)^{-1} \qquad \chi \equiv \sqrt{4D\tau} \tag{31}$$

Using τ and χ, we can define dimensionless variables, t_r, x_r and c' as,

$$t_r \equiv \frac{t}{\tau} \qquad x_r \equiv \frac{x}{\chi} \tag{32}$$

and

$$c' \equiv \frac{c}{c_{eq}} \tag{33}$$

The result is the following solution in dimensionless form:

$$c'(x_r, t_r) = (c_o' - 1)e^{-(2-\alpha)x_r} + 1 + \frac{e^{-t_r}}{\sqrt{\pi t_r}} \int_0^\infty [c'(u, 0) - (c_o' - 1)e^{-(\alpha+2)u} - 1]e^{-\alpha(u-x_r)} \cdot [e^{-(u-x_r)^2/t_r} - e^{-(u+x_r)^2/t_r}]du \quad (34)$$

The only parameter in eq (34) is the characteristic dimensionless number, α, which has been defined by

$$\alpha \equiv \frac{v\sqrt{\tau}}{\sqrt{D}} = \frac{2}{\left(1 + \frac{4Dk_{eff}}{v^2}\right)^{1/2}} \quad (35)$$

As we will see below, α measures whether flow or diffusion/dispersion dominates in the transport process; however, note that k_{eff} enters into the equation for α.

Values of α range from 0 (for $4Dk_{eff}/v^2 \gg 1$) to 2 (for $4Dk_{eff}/v^2 \ll 1$). α values near 2 indicate flow-dominated systems, whereas α values less than 1 indicate diffusion-dominated or dispersion-dominated systems.

Figure 5 illustrates the shape of the concentration profile as a function of time and the approach toward the steady state profile using reduced variables for different values of α. Low values of α yield smoothly varying curves (for example, fig. 5A and B), indicative of diffusion or dispersion domination. However, as α approaches the value 2 (fig. 5C and D) a dramatic change toward curves exhibiting flow **fronts** takes place; such fronts are typical of fluid flow dominated behavior.

The time it takes the system to reach steady state for low α (for example $\alpha = 0.1$) is around 1 to 2 in t_r, units, that is

$$t \sim 2\tau = \frac{2}{k_{eff} + \frac{v^2}{4D}} \sim \frac{2}{k_{eff}}$$

The last approximation follows from $\alpha = 0.1$, which indicates that $v^2/4D \ll k_{eff}$. On the other hand, for high values of α, (for example $\alpha = 1.90$), t_r, needs to be around 20 (see fig. 5C) to reach steady state, that is

$$t_{st} \sim 20\tau = \frac{20}{\left(k_{eff} + \frac{v^2}{4D}\right)}$$

But, if $\alpha = 1{,}90$, according to eq (35)

$$\frac{v^2}{4D} \sim 10k_{eff}$$

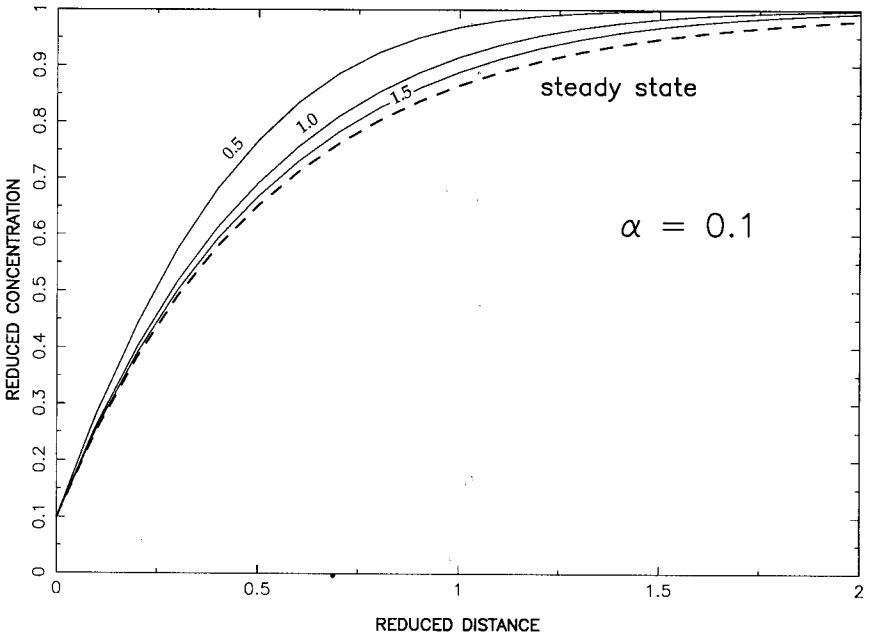

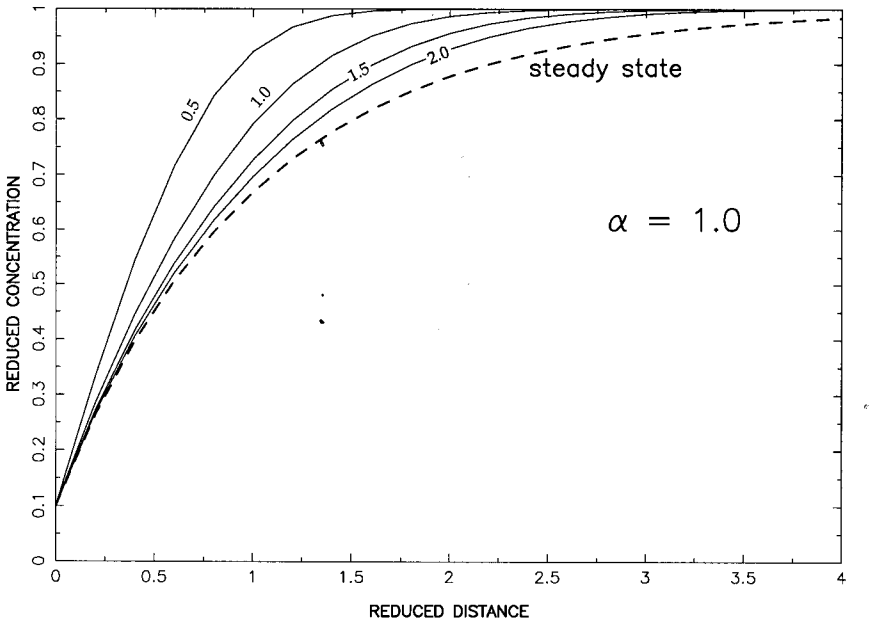

Fig. 5. Time-space evolution of the diffusion/dispersion-flow-chemical reaction model discussed in the text for different values of the parameter α. The numbers on each of the solid curves in the diagrams refer to the values of the reduced time (t_r) The dashed lines represent steady state. (A) is for α = 0.1 (diffusion dominated), (B) is for α = 1.0 (mixed).

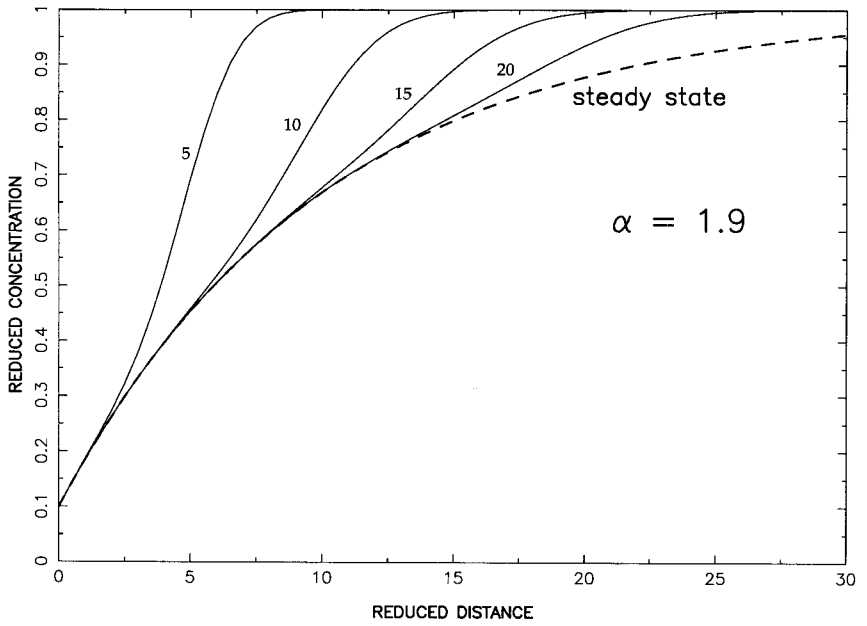

C.

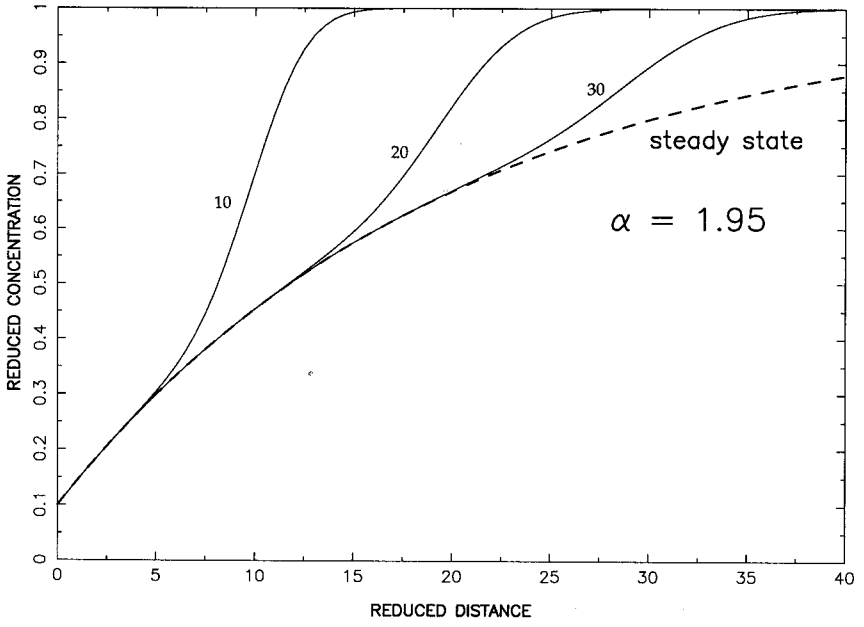

D.

(C) is for $\alpha = 1.9$ (flow dominated), and (D) is for $\alpha = 1.95$ (flow dominated).

Hence,

$$\frac{20}{\left(k_{eff} + \frac{v^2}{4D}\right)} \sim \frac{2}{k_{eff}}$$

In fact, over the entire range of α, the time needed to reach steady state ranges from $1.0/k_{eff}$ for $\alpha = 0.1$ (or 0.01, 0.001, et cetera) to $3.0/k_{eff}$ for α values between 1.8 and 2.0. Consequently, over the entire range of α, the time needed to reach steady state may be taken as:

$$t_{st} \sim \frac{2}{k_{eff}} \tag{36}$$

At steady state, according to eq (30), the distance over which the concentration profile will differ significantly (by greater than 5 percent) from equilibrium is given by:

$$\Delta x_{non\text{-}equil} \sim \frac{3}{S}$$

where S is given by eq (28). Simplifying S in the limit of high and low v,

$$\Delta x_{non\text{-}equil} \sim v\frac{3}{k_{eff}} \qquad \frac{4Dk_{eff}}{v^2} \ll 1 \tag{37}$$

$$\Delta x_{non\text{-}equil} \sim \sqrt{\frac{9D}{k_{eff}}} \qquad \frac{4Dk_{eff}}{v^2} \gg 1 \tag{38}$$

These last two equations are the same as would be obtained for the convective and diffusive (dispersive) distances traversed in a time t_{st}. Note that this non-equilibrium zone is at steady state and so will be maintained as long as the minerals are reacting, that is, as long as no one reactant is consumed totally.

Petrologic reaction kinetics.—One of the most critical needs in metamorphic petrology is the extraction of reaction kinetic data. As will be shown, the kinetic effects can be significant enough to warrant a serious attack on this problem. One of the basic kinetic questions concerns the functional *form* of the rate law (Lasaga, 1986). Wood and Walther (1983) and Walther and Wood (1984) used essentially a *linear* approach, which is based on transition state theory arguments (see, for example, Lasaga, 1981). However, it is not certain that metamorphic reactions will, in general, behave in this fashion (see, for example, Lasaga, 1986).

To model the chemical evolution of a metamorphic rock + fluid system, it is necessary to specify the form of the rate law, R_j (*moles/cm*^{3} *fluid/yr*), applicable to the *jth* reaction in a metamorphic assemblage. These R_j are the terms needed in eqs (4), (5), (6). In addition, to apply the general results from the kinetic models of the previous sections, these R_j,

obtained from petrologic experimental kinetic data, must be recast in the form used in eqs (13) and (19). There are many possible rate expressions for R_j. Only careful experimental work will determine the correct R_j rate laws relevant to the important metamorphic reactions. Based on earlier work in heterogeneous kinetics, a useful general rate law can be written as:

$$R_j = k_j A_j \Delta G_j^{n_j} / \phi \tag{39}$$

where k_j is an intrinsic rate constant ($moles/cm^2/yr/(cal/mole)^{n_j}$), A_j is the **specific area** of the limiting mineral (Lasaga, 1986) for the *jth* reaction ($cm^2/cm^3\ rock$), ΔG_j is the free energy change for the *jth* reaction ($cal/mole$), ϕ is the porosity, and n_j is the order of the reaction. k_j is termed *intrinsic* because the important dependence on both surface areas (extensive) and the free energy of reaction have been factored out. While k_j may still depend on a variety of other factors (for example, catalysts or inhibitors), k_j will have a very strong temperature dependence which will usually follow an Arrhenius expression:

$$k_j = k_j^0 e^{-\frac{E_{a,j}}{R}\left(\frac{1}{T} - \frac{1}{T_0}\right)} \tag{40}$$

$E_{a,j}$ is the activation energy of the reaction and can be several tens of *Kcal/mole*. Eq (40) has been written such that k_j^0 is the value of the rate constant at some reference temperature, T_0.

Eqs (39) and (40) single out five major variables in the kinetic description of metamorphic reactions:

1. Specific surface area (texture)
2. Temperature
3. Deviation from equilibrium (ΔG)
4. Porosity
5. Order of the reaction (linear or non-linear)

The specific surface area term in eq (39) is a crucial parameter in predicting the kinetic behavior of mineral assemblages. The specific surface area of any one mineral will depend on the abundance and the shape of the mineral grains. The surface area needed in eq (39) also requires that the surface be in contact with the fluid. The models used to obtain the reactive mineral surface area will then depend on both the rock texture and the mode of transport of the fluid (for example, whether it is pervasive flow or flow through fractures). In addition, the actual mineral surface area that limits the rate of the *jth* reaction may vary as reactants are used or products are formed (Lasaga, 1986). In simple cases, the limiting surface area will be determined by the minerals that have both low surface area and slow surface reaction kinetics.

If the shape of mineral grains for any one mineral, θ, could be approximated by a sphere, then the specific surface area of the mineral,

A_θ, can be evaluated from the mineral abundance, N_θ (*number of crystals/cm³ rock*), and the mineral radius, r_θ:

$$A_\theta = 4\pi r_\theta^2 N_\theta \tag{41}$$

N_θ may also be obtained from the volume percent abundance of the mineral, x_θ, and the mean size, r_θ, according to

$$N_\theta = \frac{3x_\theta}{400\pi r_\theta^3} \tag{42}$$

(Lasaga, 1984). The area predicted by eq (41) can vary by several orders of magnitude in natural assemblages.

One of the biggest factors affecting the surface area of a mineral is the nucleation rate. Our knowledge of nucleation rates in metamorphism is very poor. The usual way to circumvent this problem is to assume that the number of nuclei, N_θ, is constant (for example, eq 42) and to vary the radius. For a mineral not initially present, N_θ is not zero, but r_θ is set to zero.

The radius needed in eq (41) must be updated throughout the modeling of a metamorphic event. Because some minerals begin at "zero" radius (they are not present), the change in radius is computed from the predicted change in volume of the mineral as given in the following equation:

$$\frac{4}{3}\pi r_{i,new}^3 - \frac{4}{3}\pi r_{i,old}^3 = \sum_{j=1}^{n_r} \frac{\overline{V}_i \nu_{ij} R_j \Delta t}{N_i} \tag{43}$$

where $\overline{V}_i$ is the ith mineral molar volume (*cm³/mole*), ν_{ij} is the stoichiometric coefficient of mineral i in the *jth* reaction, R_j is the net rate of the *jth* reaction, and Δt is the time step used in the numerical scheme.

As an example of a set of metamorphic reactions, table 2 gives a set of reactions relevant to metamorphism in the Marysville contact aureole (Rice, 1977). The free energy change for the n_r reactions in table 2 is computed in the standard way:

$$\Delta G_j = \Delta G_j^0(P, T) + \nu_{H_2O,j} RT \ln (f_{H_2O}) + \nu_{CO_2,j} RT \ln (f_{CO_2}) \tag{44}$$

Values for the standard Gibbs free energies are computed from the expressions given in Rice (1977):

$$-\frac{\Delta G_j^0}{\ln (10) RT} = \frac{A_j'}{T} + B_j' + \frac{C_j(P-1)}{T} \tag{45}$$

where A', B', and C are constants obtained from thermodynamic data and given in Rice (1977) for each of the reactions.

TABLE 2

Metamorphic reactions

1.	3Do + Ksp + H_2O = Phl + 3Cc + 3CO_2
2.	5Do + 8Q + H_2O = Tr + 3Cc + 7CO_2
3.	Phl + 2Do + 8Q = Tr + Ksp + 4CO_2
4.	5Phl + 6Cc + 24Q = 3Tr + 5Ksp + 6CO_2 + 2H_2O
5.	Do + 2Q = Di + 2CO_2
6.	Tr + 3Cc + 2Q = 5Di + 3CO_2 + H_2O
7.	Tr + 3Cc = 4Di + Do + CO_2 + H_2O
8.	3Tr + 6Cc + Ksp = Phl + 12Di + 6CO_2 + 2H_2O
9.	Tr + 2Do + Ksp = 4Di + Phl + 4CO_2
10.	Tr + 11Do = 8Fo + 13Cc + 9CO_2 + H_2O
11.	Di + 3Do = 2Fo + 4Cc + 2CO_2
12.	3Tr + 5Cc = 11Di + 2Fo + 5CO_2 + 3 H_2O

Cc = calcite Do = dolomite Q = quartz Tr = tremolite
Di = diopside Fo = forsterite Ksp = K-feldspar Phl = phlogopite

The fugacities are computed assuming the Lewis and Randall rule:

$$f_j = X_j f_j^0 \tag{46}$$

The fugacities of the pure gases, f_j^0, were obtained from the data of Burnham, Holloway, and Davis (1969) and Skippen (1974) by fitting the tables to a series of the form

$$f_j^0 = \sum_i a_i T^i \tag{47}$$

for a particular pressure. Use of eq (47) will be needed later in the paper for detailed simulations monitoring many variables at once. a_i values for 1 *kb* are given in table 3.

TABLE 3

Fugacity terms a_i at 1 kb

	H_2O
i	a_i
0	992.9840
1	−9.44161
2	0.0310854
3	-3.585861×10^{-5}
4	1.434484×10^{-8}
	CO_2
i	a_i
0	195.4298
1	4.867755
2	−0.00674962
3	3.111111×10^{-6}

The values of n_j and k_j needed in the general eq (39) are not known for most metamorphic reactions. There have been several recent studies on the kinetics of high and medium grade metamorphic reactions. Typically, the experiments have used powdered samples with abundant fluid present. Most of these experiments have shown that the metamorphic reactions are surface controlled. It is important to stress that, for our purposes, use of these rate constants is perfectly adequate. The only scenario in the field that would alter the rate of the metamorphic reactions from the laboratory values would be one where diffusion along grain boundaries is exceedingly slow. In this case, the rate would be slower than the laboratory rate. Therefore, deviations from equilibrium calculated in this paper using laboratory data can only be exacerbated by this diffusion scenario. With this argument in mind, the kinetic data on the dehydration of muscovite from Schramke, Kerrick, and Lasaga (1987) can be used as a useful guideline. If a first order reaction is assumed, $n_j = 1$, and the 2 *kb* data can be used to obtain k_j at 600°C:

$$k_j^0 = \frac{10^{-12}\ moles/cm^2/sec}{3000\ Joules/mole}$$

or with time in years and energy in *cal/mole,*

$$k_j^0 = 4 \times 10^{-8}\ \frac{moles/cm^2/yr}{cal/mole} \tag{48}$$

On the other hand, based on the **non-linear rate law** discussed in Lasaga (1986):

$$R_j = 4.38 \times 10^{-22} \Delta G^{2.68}\ moles/cm^2/sec$$

where ΔG is in *Joules/mole* or

$$R_j = 6.4 \times 10^{-13} \Delta G^{2.68}\ moles/cm^2/yr$$

with time in years and ΔG in *cal/mole.* Therefore, in the non-linear case:

$$k_j^0 = 6.4 \times 10^{-13}\ \frac{moles/cm^2/yr}{(cal/mole)^{2.68}} \tag{49}$$

$$n = 2.68$$

where $t_0 = 600$°C once more.

To apply the previous models to our metamorphic terrane, we need to evaluate the k_{eff} in eqs (13) or (19). To do this for linear kinetics, we must convert the term:

$$\frac{k_j A_j \Delta G_j}{\phi}$$

to the term $k_{eff}(c_{eq} - c)$. Near equilibrium, we may use a Taylor series, at any given temperature to write

$$\Delta G_j = \frac{\partial \Delta G_j}{\partial c}(c - c_{eq})$$

As a result,

$$k_{eff} = \frac{k_j A_j}{\phi}\frac{\partial \Delta G_j}{\partial c}$$

Using eq (44) we obtain:

$$k_{eff} = \frac{k_j A_j}{\phi} RT_{eq}\left[\frac{\nu_{CO_2}}{X^{eq}_{CO_2}} - \frac{\nu_{H_2O}}{1 - X^{eq}_{CO_2}}\right]\frac{\partial X_{CO_2}}{\partial c_{CO_2}} \tag{50}$$

or

$$k_{eff} = \frac{k_j A_j}{\phi} RT_{eq}\left[\frac{\nu_{CO_2}}{X^{eq}_{CO_2}} - \frac{\nu_{H_2O}}{1 - X^{eq}_{CO_2}}\right]\frac{\overline{V}^2}{\overline{V}_{H_2O}} \tag{51}$$

If we use an area of $A = 1.5\ cm^2/cm^3\ rock$ (for example, 5 percent volume abundance and $r = 1\ mm$ in eqs (41) and (42)), $\phi = 0.001$, $k = 4 \times 10^{-10}$ *moles/cm*^{2}*/yr/(cal/mole)*, $T_{eq} = 400°C$, $P = 1kb$, $X^{eq}_{CO_2} = 0.4$, $\nu_{CO_2} = 3$, $\nu_{H_2O} = -1$ (using reaction (1) in table 2), $\overline{V}_{CO_2} = 68.3\ cm^3/mole$, and $\overline{V}_{H_2O} = 18.7 cm^3/mole$, we obtain

$$k_{eff} = 0.585\ yr^{-1}$$

Given this value of the rate constant, eq (36) predicts that the time needed to achieve a steady state will be:

$$t_{st} = \frac{2}{0.585} = 3.4\ yrs$$

If $\nu_{CO_2} = 1$, then the same calculation would yield $k_{eff} = 0.265\ yr^{-1}$ and $t_{st} = 7.5\ yrs$. The importance of this time to possible models of natural systems depends on the frequency of variation of other processes. If the movement of fluids and the thermal evolution proceed at a uniform pace—on the time scale of 100 *yrs*—then a steady state will be achieved.

We can use the value of k_{eff} ($0.585\ yr^{-1}$) to determine also whether diffusion or transport will dominate the metamorphic region. If the value of the diffusion and dispersion coefficient is taken as $D = 0.031\ m^2/yr$ (note that this value could increase by 1 or 2 orders of magnitude if dispersion is bigger) we have:

$$\frac{4Dk_{eff}}{v^2} = 7.4 \qquad (v = 0.1\ m/yr) \tag{52}$$

$$\frac{4Dk_{eff}}{v^2} = 0.07 \qquad (v = 1.0\ m/yr) \tag{53}$$

Therefore, the transition between diffusion control and transport control occurs between flow values of 0.1 and 1.0 *m/yr*. These flow values are, in fact, not atypical of values estimated from solution to the flow equations in a hydrothermally driven system at low pressure (several kilobars) (Cathles, 1977). As additional examples of typical fluid flow rates, we can use data from Ferry (1991). Even though he used an equilibrium model, Ferry calculated integrated fluid fluxes of 1000 *moles/cm²* for a variety of plutons several *kilometer* in diameter. The typical cooling period for these types of plutons is 10^5 to 10^6 *yrs*. If we use 5×10^5 *yrs* the flow rate becomes 2000 *moles/cm²*/10^6 *yrs*. Using a fluid density of 0.5 *g/cm³* this flow translates to a Darcy flow of 0.07 *cm/yr*. In fact, recall that the velocities important in this paper are the *true* velocities that equal v_{Darcy}/ϕ. Assuming a porosity ϕ of 0.001 yields a true velocity of 0.7 *m/yr*. As these calculations assume a chemical equilibrium model the true velocity v could be much larger. For this value of k_{eff} (0.585 yr^{-1}), the non-equilibrium distance will be

$$\Delta x_{non\text{-}equil} = 0.72\ m \qquad (v = 0.01\ m/yr) \tag{54}$$

$$\Delta x_{non\text{-}equil} = 1.00\ m \qquad (v = 0.10\ m/yr) \tag{55}$$

$$\Delta x_{non\text{-}equil} = 5.2\ m \qquad (v = 1.0\ m/yr) \tag{56}$$

$$\Delta x_{non\text{-}equil} = 51\ m \qquad (v = 10.0\ m/yr) \tag{57}$$

$$\Delta x_{non\text{-}equil} = 513\ m \qquad (v = 100.0\ m/yr) \tag{58}$$

The values of $\Delta x_{non\text{-}equil}$ shown in eqs (54) to (58) were calculated assuming that the diffusion/dispersion coefficient was only 10^{-5} *cm²/sec* (0.031 *m²/yr*). At high temperatures and/or if dispersion is important the diffusion/dispersion coefficient could attain values as large as 0.01 *cm²/sec*. For this value of D the non-equilibrium distances for the same value of k_{eff} will be

$$\Delta x_{non\text{-}equil} = 22\ m \qquad (v = 0.01\ m/yr) \tag{59}$$

$$\Delta x_{non\text{-}equil} = 22\ m \qquad (v = 0.10\ m/yr) \tag{60}$$

$$\Delta x_{non\text{-}equil} = 25\ m \qquad (v = 1.0\ m/yr) \tag{61}$$

$$\Delta x_{non\text{-}equil} = 59\ m \qquad (v = 10.0\ m/yr) \tag{62}$$

$$\Delta x_{non\text{-}equil} = 514\ m \qquad (v = 100.0\ m/yr) \tag{63}$$

Note the importance of transport in determining the thermodynamic scenario of the metamorphic terrane! Obviously, high flow rates and low k_{eff} lead to quite large deviations from equilibrium. However, even for low flow rates the presence of diffusion leads to significant non-equilibrium distances. The magnitude of k_{eff} depends on a large number of variables as illustrated in eq (51). Note that even though k_{eff} was such that the time needed to achieve steady state was geologically short, the spatial extent of disequilibrium in the steady state could be geologically very significant. The results shown in eqs (54) to (63) will play

a key role in changing our usual way of thinking about paths in metamorphic events!

In the case of non-linear kinetics, we must convert the term:

$$\frac{k_j A_j \Delta G_j^n}{\phi}$$

to the term $k'(c_{eq} - c)^n$. Using a similar treatment as used in the linear case and the relation $k_{eff} = k' c_{eq}^{n-1}$, k_{eff} for the non linear case is given by:

$$k_{eff} = \frac{k_j A_j}{\phi}\left[\frac{\nu_{CO_2}}{X^{eq}_{CO_2}} - \frac{\nu_{H_2O}}{1 - X^{eq}_{CO_2}}\right]^n (RT_{eq})^n \frac{\overline{V}^{n+1}}{\overline{V}^{n}_{H_2O}} X^{eq}_{CO_2}{}^{n-1} \qquad (64)$$

where, regardless of the value of n, k_{eff} has units of inverse time.

Using the value of n from eq (49) and reducing k_j for a temperature of 400°C leads to

$$k_j = 6.4 \times 10^{-15} moles/cm^2/yr/(cal/mole)^{2.68} \qquad n = 2.68 \qquad (65)$$

If $A = 1.5\ cm^2/cm^3\ rock$, $\phi = 0.001$, $T_{eq} = 400°C$, $P = 1kb$, $X^{eq}_{CO_2} = 0.4$, $\nu_{CO_2} = 3$, $\nu_{H_2O} = -1$, $\overline{V}_{CO_2} = 68.3\ cm^3/mole$, and $\overline{V}_{H_2O} = 18.7\ cm^3/mole$, and if we use the values of k_j and n in eq (65) then use of eq (64) results in

$$k_{eff} = 50.04\ yr^{-1} (\nu_{CO_2} = 3,\ \nu_{H_2O} = -1) \text{ (see table 2)}$$

and

$$k_{eff} = 6.05\ yr^{-1} (\nu_{CO_2} = 1,\ \nu_{H_2O} = -1) \text{ (see table 2)}$$

These values can now be inserted into the earlier eq (23) to obtain the non-equilibrium distances. Therefore, for the case $\nu_{CO_2} = 3$, $\nu_{H_2O} = -1$

$$\Delta x_{non\text{-}equil} = 3\ m \qquad (v = 1\ m/yr)$$
$$\Delta x_{non\text{-}equil} = 27\ m \qquad (v = 10\ m/yr)$$
$$\Delta x_{non\text{-}equil} = 270\ m \qquad (v = 100\ m/yr)$$

Similarly for the case that $\nu_{CO_2} = 1$, $\nu_{H_2O} = -1$

$$\Delta x_{non\text{-}equil} = 23\ m \qquad (v = 1\ m/yr)$$
$$\Delta x_{non\text{-}equil} = 225\ m \qquad (v = 10\ m/yr)$$
$$\Delta x_{non\text{-}equil} = 2250\ m \qquad (v = 100\ m/yr)$$

Therefore, even though the kinetics of closed systems may be fast on a laboratory time scale, the extent of significant disequilibrium can be quite extensive, and furthermore, the distance will be quite sensitive to non-linearities in the rate law.

The importance of steady state in significantly modifying the models of fluid-rock interaction in metamorphism can be gleaned from the

calculations discussed above. It is essential to point out that the non-trivial role played by steady state applies both to contact and to regional metamorphism and that the lack of equilibrium can be maintained for tens of thousands or tens of millions of years, because the time scale now is following the time scale for the disappearance of some of the racting minerals. Note that in any terrain with different length scales for reacting assemblages, the spatial scale for non-equilibrium steady state, $\Delta x_{non\text{-}equil}$, may be such that no part of the system achieves local equilibrium even on a scale of millions of years. For instance, figure 6 illustrates the case where fluid flow is across lithologic boundaries, and $\Delta x_{non\text{-}equil}$ is larger than the width of individual lithologic units. Yet, it should be reiterated, this situation could arise with an intrinsic reaction rate constant that leads to half-lives in a closed system of only 10 *yrs*.

EVIDENCE FOR NON EQUILIBRIUM IN THE MARYSVILLE AUREOLE

In most, if not all, petrologic and isotopic studies, it has been assumed that local chemical and isotopic equilibrium were achieved. Yet, in the combined isotopic and mixed volatile equilibria study of Lattanzi, Rye, and Rice (1980) they showed that it was not possible to interpret the data to indicate that both isotopic and chemical equilibria were achieved.

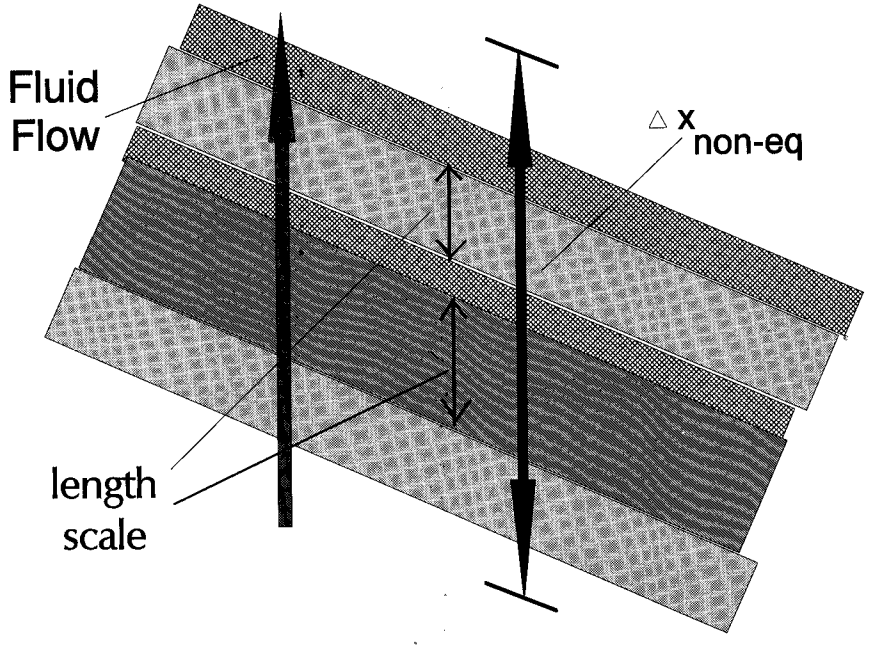

Fig. 6. Sketch showing relations between the different length scales of lithologic units and $\Delta x_{non\text{-}equil}$. In these cases, the system may never reach equilibrium.

This result requires us to modify the equilibrium assumptions often made in petrologic and isotopic models.

The fundamental problem at Marysville between the petrologic and isotopic data is illustrated in figures 7 and 8 (figs. 1, 2, and 3 of Lattanzi, Rye, and Rice, 1980). Figure 7 summarizes the interpretation of the petrologic and field data presented by Rice (1977). Figure 8 presents the carbon and oxygen isotopic results on carbonates determined by Lattanzi, Rye, and Rice (1980).

Rice (1977) was able to demonstrate that the petrologic and field relationships observed for rocks from low and intermediate grades in the phase volume Cc–Do–Q–Ksp could be interpreted to represent a system in which the fluid compositions were buffered along isobaric univariant reactions with little or no addition of externally derived fluid. In fact, he was able to demonstrate that both the sequence of isograds and the spacing between isograds could be reproduced if the fluids followed the path shown in figure 7B. As further evidence for this behavior, he was able to show that calcite-dolomite solvus temperatures corresponded to the predicted temperatures along path II-III, and that the calcite compositions are consistent with equilibrium within the assemblage tremolite–calcite–quartz.

The isotopic data (fig. 8) exhibit a large depletion in both ^{13}C and ^{18}O for carbonate remaining in the low variant mineral assemblages. As the only carbon reservoir in the rock is carbonate and a large fraction of the original carbon was lost from the rock during decarbonation reactions, the ^{13}C depletion can be explained by continuous loss of the CO_2 that was in local isotopic equilibrium with the carbonate during decarbonation (Rayleigh distillation). On the other hand, the ^{18}O data cannot be explained in the same simple manner because only two-thirds of the carbonate oxygen is lost during decarbonation and because the majority of the oxygen in the rock is in the reactant and product silicates.

The problem is that the oxygen isotopic data require that either:

1. There were kinetic isotopic effects on the oxygen isotope values of the carbonates.
2. The equilibrium model used by Rice (1977) and many other petrologists does not apply.
3. Both of the above.
4. The oxygen isotopic systematics were not established at the same time as the phase and chemical systematics.
5. An external fluid was added that had the same X_{CO_2} as the fluids produced by the fluid buffer reactions. That is, the fluid had a composition nearly identical to the fluid composition at which most of the reaction took place in the Rice (1977) scenario (the isobaric invariant and singular points).

Lattanzi, Rye, and Rice (1980) rejected (4) because the amount of ^{18}O depletion appeared to be related to the amount of reaction that had taken place in the rock. They rejected (5) because it seemed highly unlikely that the X_{CO_2} of the external fluid would be exactly or almost

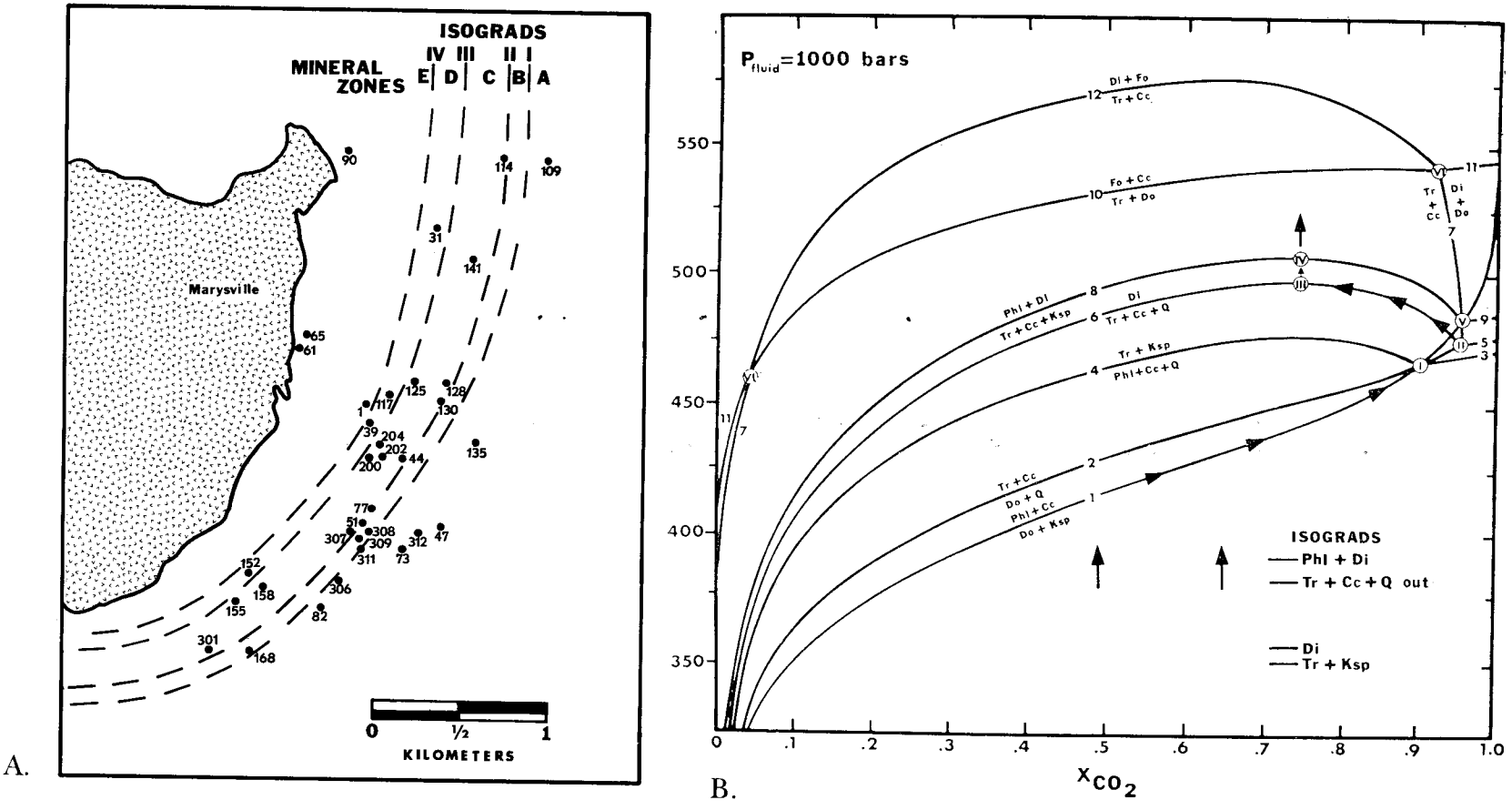

Fig. 7(A) Isograds for the Marysville contact aureole from Rice (1977). (B) Phase diagram with inferred reaction path for the Marysville contact aureole (Rice, 1977).

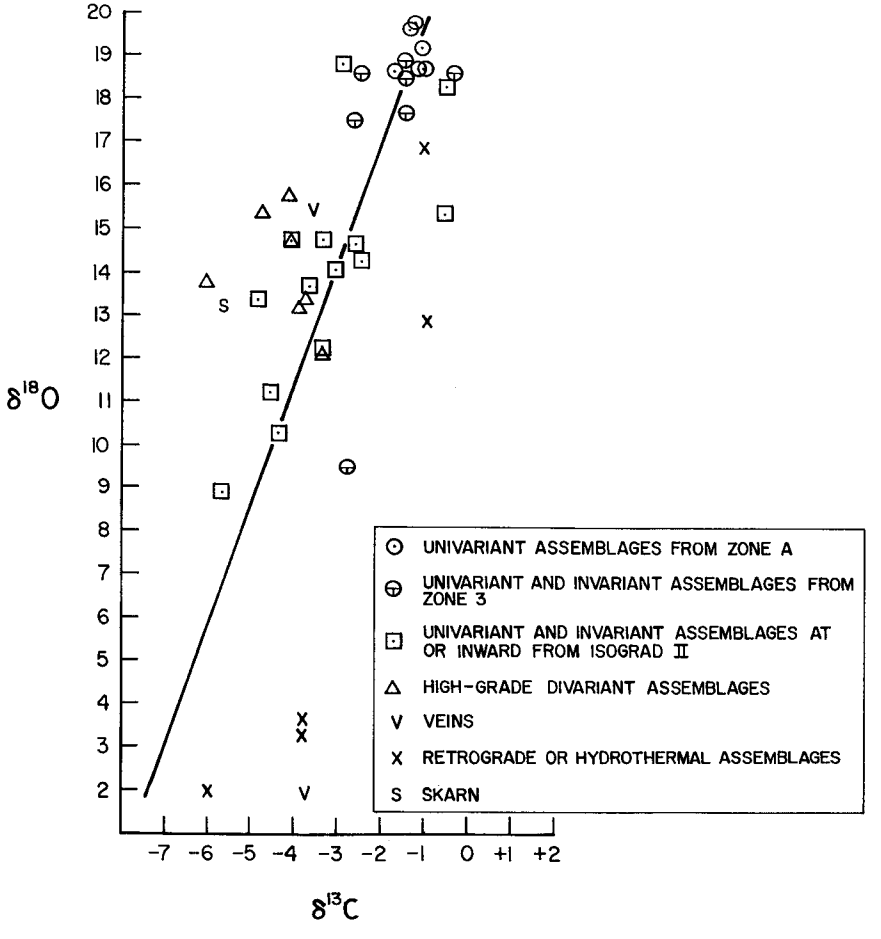

Fig. 8. $\delta^{13}C$ and $\delta^{18}O$ data for carbonates from the Marysville aureole (Lattanzi, Rye, and Rice, 1980).

exactly the same as the fluid produced at the apparent isobaric invariant point. They suggested that the oxygen isotopic data could be explained if the carbonate-CO_2 oxygen isotope exchange was rapid, the reactant silicates-CO_2 oxygen isotope exchange was slow or non existent, and the product silicates did not back exchange with the remaining carbonate.

A major problem with the Lattanzi, Rye, and Rice (1980) interpretation of the isotopic data is seen in figure 8. The oxygen and carbon isotopic values obtained on calcites from hydrothermal veins and from skarn mineralization either overlap with the values observed in the calcites from the metamorphic assemblages, or they appear to form endmember values on the isotopic trend defined by the metamorphic

assemblage calcites. Without the "constraint" of the local equilibrium petrologic model, these data would clearly be interpreted to represent an open system that had undergone variable and large amounts of exchange with a hydrothermal fluid. This result makes it imperative for us to test whether it is possible to produce the chemical, phase, and field observations at Marysville in an open non-equilibrium system.

In the previous discussion we have demonstrated the importance of taking into account the coupling between fluid flow and the kinetics of chemical reactions in understanding the chemical evolution of reaction fronts or kinetic isograds in nature. The simple models presented earlier need to be expanded to treat a much more complex system such as that in the contact aureole at Marysville. The following section will introduce such a model and will present some initial results based on available kinetic data. It should be noted that the kinetics of several of the important reactions in the contact aureole at Marysville have already been studied (Dachs and Metz, 1988; Heinrich, Metz, and Gottschalk, 1989; Heinrich, Metz, and Bayh, 1986). We do not offer the model results as a final solution to the Marysville problem. Rather we offer them to illustrate the possible importance of kinetic effects resulting from coupling fluid flow to chemical reactions at Marysville.

MODEL

To study more complex situations than the simple models outlined earlier, numerical simulations need to be carried out. Figure 9 illustrates the model system we will use to simulate the contact aureole at Marysville. The model considers constant one dimensional fluid, in either direction, and explicitly takes into account both the spatial and temporal variations in temperature by solving the conservation of energy equation (eq 1). Furthermore, at any point in the system, the model tracks the rates of many possible reactions simultaneously, depending on the temperature, fluid composition, and mineral abundance at that point. This allows the model to follow the chemical evolution of the fluid as well as the mineral abundances by solving eqs (5) and (6). The equations are solved using an implicit finite difference method similar to that used in Lasaga (1986). We will use the reaction scheme and phase diagram topology of Rice (1977). The 12 reactions in the scheme of Rice (1977) are given in table 2. Figure 10 gives our calculated topology for the possible T-X univariant lines of this sytem, including all the metastable extensions. Figure 10 agrees closely with the results given in Rice (1977). By way of reference, figure 7B illustrates the T-X_{CO2} pathway deduced by Rice (1977). This pathway would correspond to infinite chemical reaction rates, no external flow, and no diffusion.

In a real system, the surface areas of reactant and product minerals vary as a function of both time and space in the reaction zone (that is the texture changes), this fact leads to a k_{eff} (in eq 24) that is a function of x and t. In addition to the time and space dependence of k_{eff}, k_{eff} will include contributions from all possible reactions being overstepped. Note that

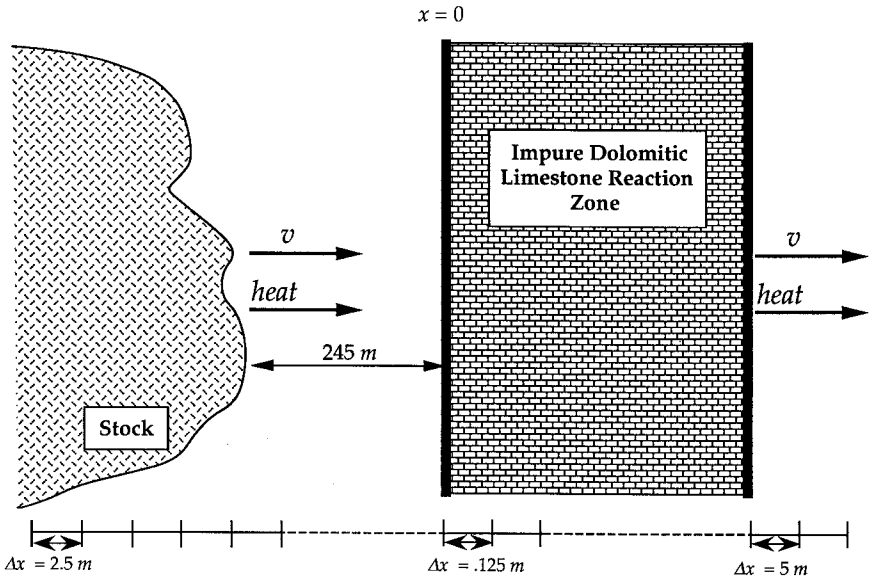

Fig. 9. Sketch of the model used to analyze the evolution of fluids in Marysville, Montana. Both fluid flow and heat flow are entering and leaving the reaction zone of impure carbonates. The reaction zone begins at a distance of 245 *m* from the contact. The grid used a spatial spacing of 2.5 *m* from the center of the stock to the reaction zone, 0.125 *m* in the zone, and 5 *m* beyond the zone.

the rate of chemical reaction for H_2O or CO_2 for the 12 reactions in table 2 is given by:

$$Rate = \sum_{j=1}^{12} \frac{R_j A_j \Delta G_j^{n_j}}{\phi}$$

where *each* reaction has its own R_j, n_j, and where A_j is the specific area of the mineral limiting the reaction. Using our notation:

$$R_{Total} = \sum_{j=1}^{12} k_{eff,j}(c - c_{eq,j}) \text{ for linear kinetics, or:}$$

$$R_{Total} = \sum_{j=1}^{12} k_{eff,j} c_{eq,j} \left(1 - \frac{c}{c_{eq,j}}\right)^{n_j} \text{ for non-linear kinetics}$$

Not only is R_{Total} used to solve for the variations of the fluid composition, c, but also the rates of the 12 individual reactions are used to change the modal abundances of the various reactant and product minerals (and therefore their areas) just as was done in Lasaga (1984).

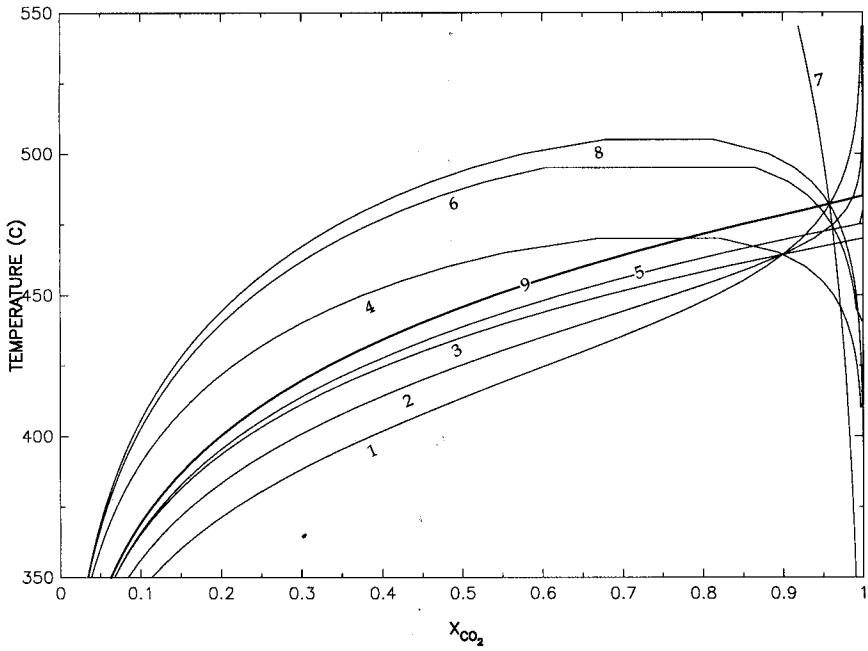

Fig. 10. T-X_{CO_2} equilibrium curves for the reactions given in table 2. Reaction curves are numbered according to the numbering scheme used in table 2.

To solve all the various equations (for example, eqs. 1, 5, 6) in an implicit finite difference scheme the distance from the center of the intrusion (heat source) to the outer fringes of the country rock was divided into small intervals, Δx, and the equations reduced to finite difference form. Because of the spatial variations in the intensity of the reactions, the size of Δx was allowed to vary, taking the smallest value in the reaction zone itself. Typically, Δx was 2.5 *m* near the contact (and in the intrusion), 0.5 *m* in the reaction zone, and 5 m beyond. Typical runs used about 1200 space intervals. The time step employed in solving the finite difference equations was found to be stable at around 0.125 *yr*, although again the program allowed for time step changes. The fluid flow was assumed to be in the direction of heat transport. The authors are aware that the flow direction could be in the opposite direction or even change in time (Furlong, Hanson, and Bowers, 1991). Nonetheless, the main conclusions reached regarding overstepping equilibrium will apply for all cases involving fluid flow.

The reaction zone begins 245 *m* from the contact with the intrusion and ends 745 m (or greater if need be) from the contact. This simplification enables a boundary condition of fixed X_{CO_2} to be maintained beyond

the reaction zone. Such a boundary condition is not unreasonable, because it represents the edge of a "reaction front" at some particular time. For example, if the reaction were the dehydration of muscovite and the entire country rock had a uniform muscovite content, it would still be true that some time after the intrusion all the muscovite would be removed up to some distance from the contact (Lasaga, 1986). The reaction rate was arbitrarilty set to zero below 300°C and above 300°C followed eqs (39) and (40). The heat flux was driven by introduction of an intrusion, and the typical half-width of the intrusion was taken to be 1 *km*. The volume abundances and mean radii used for the various mineral phases are given in table 4. Values of κ, D, ϕ, and v used are given in table 5.

The value of E_a in eq (40) is not well known. Based on low temperature silicate-water reactions it could be in the vicinity of 15 *kcal/mole* (Lasaga, 1984). However, based on a wider range of silicate reactions, the activation energy could be from 15 *kcal/mole* to 70 *kcal/mole*. In fact, Schramke, Kerrick, and Lasaga (1987) obtained a range of E_a from 10 *kcal/mole* to 60 *kcal/mole* in their work on muscovite dehydration. In the simulations that follow, E_a was left at the lower (conservative) value of 20 *kcal/mole*. This activation energy is also consistent with the data from Dachs and Metz (1988), Heinrich, Metz, and Bays (1986), and Heinrich, Metz, and Gottschalk (1989). However, to compensate for varying (higher) activating energies, the k value of 500°C was varied from 4×10^{-8} to 4×10^{-11} *moles/cm²/yr/(cal/mole)*. Remember that Schramke, Kerrick, and Lasaga (1987) obtained a k value for the muscovite dehydration reaction of 4×10^{-8} at 600°C. With the uncertainties in E_a this value translates into a range in k of 9×10^{-9} to 4×10^{-10} *moles/cm²/yr/(cal/mole)* at 500 °C. The same treatment for the data, obtained on reaction 10 in table 2, from Heinrich, Metz, and Gottschalk, (1989), yields a range of 4×10^{-9} to 2×10^{-11} *moles/cm²/yr/(cal/mole)* assuming linear kinetics within the range of ΔG from 0 to 10 *kcal/mole*.

MODEL RESULTS

Figures 11 to 18 present the initial results of applying our model to the Marysville setting. These figures point out the importance of the

TABLE 4

Mineral volume abundances and mean radii

Mineral	x_θ(v. %)	r_θ(cm)
Calcite	20	0.05
Quartz	10	0.10
Dolomite	40	0.05
K-feldspar	5	0.10
Phlogopite	5	0.05 (0)
Tremolite	5	0.10 (0)
Diopside	5	0.10 (0)
Forsterite	5	0.10 (0)

*Number given is used to determine N_θ for the minerals not initially present.

TABLE 5

Physical constants used in calculations

Property	Value
Fluid flow v	0.01-0.1 m/yr
Diffusion coefficient D	0.0315 m^2/yr
Thermal diffusivity κ	0.01 cm^2/yr
Porosity ϕ	0.001

nature and degree of overstepping possible within reasonable variations in the parameters of the model. In particular the figures concentrate on the effect of varying the rate constant k_j^0, the flow rate v, the porosity ϕ, and the mineral abundances. The figures analyze the evolution of the fluid composition both as a function of time for a fixed location (that is a T-X_{CO_2} path) and for a given time as a function of distance throughout the aureole. The latter variation reflects the non-equilibrium distances discussed earlier in the paper.

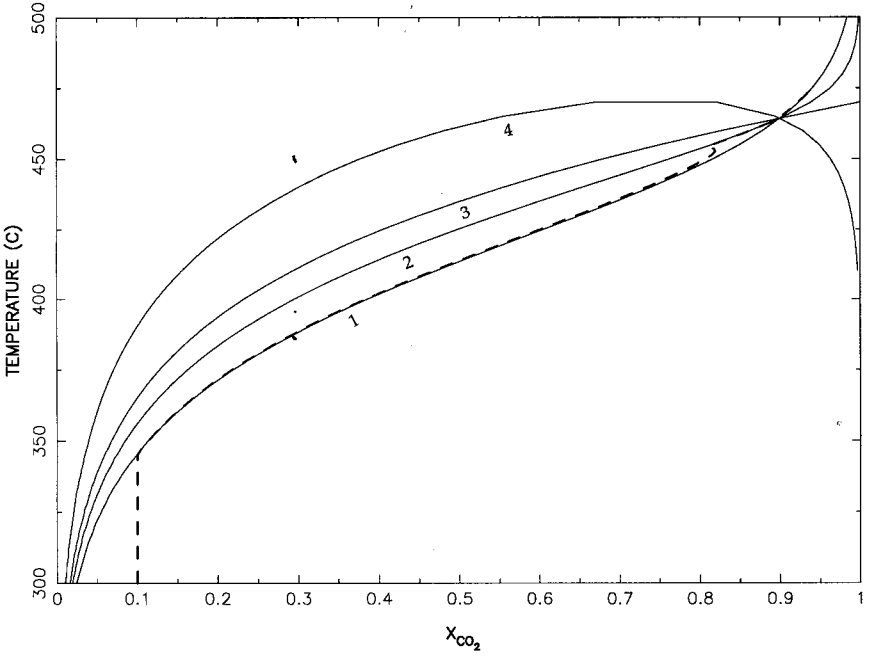

Fig. 11. T-X_{CO_2} evolution diagram for a rock sample 750 m from the contact and for the case $k_j^0 = 4 \times 10^{-8}$ $moles/cm^2/yr/(cal/mole)$ and for a fluid flow rate of $v = 0.01$ m/yr. The other variables are given in tables 4 and 5 and in figure 10. Note that for the initial mineral abundances chosen, feldspar was used up before the invariant point was reached.

Figures 11 through 13 illustrate the effect varying k_j^0 in eq (40) has on the predicted reaction path of the system at a fixed point in space. The reaction paths shown in figures 11, 12, and 13 were obtained by following the T and X_{CO_2} evolution at a fixed point in the reaction region and by plotting the variations with time. The position used in each of these figures was 750 m from the contact with the intrusion. Using $k_j^0 = 4 \times 10^{-8}$ *moles/cm²/yr/(cal/mole)* and $\phi = 0.001$ yields the results shown in figure 11. Note that the T-X_{CO_2} pathway, in this case, follows closely that in figure 7B, and that the equilibrium assumption is reasonable. However, it is quite possible to encounter higher E_a and lower k_j^0 as well as higher ϕ. Figure 12 illustrates the results of lowering k_j^0 to 4×10^{-9} and 4×10^{-10} *moles/cm²/yr/(cal/mole)*, respectively. Note that in figure 12A there is a slight deviation from the expected path. On the other hand, the results in figure 12B indicate a serious deviation from the usual path, and the system crosses two metastable reactions.

Figure 13 illustrates some of the scenarios that can develop with having different rates for different reactions. In the calculation of figure 13A a value of $k_1^0 = 4 \times 10^{-11}$ *moles/cm²/yr/(cal/mole)* was used while the rates of reactions 2 and 3 were kept arbitrarily to zero such that the limiting surface area was that of tremolite for both reactions. Note in this case three metastable reactions were crossed. Figure 13B illustrates the case where reaction 1 is relatively slow ($k_1^0 = 4 \times 10^{-11}$ *moles/cm²/yr/(cal/mole)* and reactions 2, 3, and 4 are all possible with a fast reaction for reaction 2 ($k_2^0 = 4 \times 10^{-8}$ *moles/cm²/yr/(cal/mole)*. Now the system oversteps reaction 1 but then proceeds to follow the metastable reaction 2 closely. It is important to stress that the kinetic variables used in the results of figure 13 can be easily derived from the experimental data of the muscovite dehydration reaction. The experiments were carried out in the laboratory and were measurable. Yet, the fact that the experiments can take place in the laboratory does not automatically lead to the usual assumption that the rates are infinitely fast in the field (Lasaga, 1989)!

The results of figure 12 and 13 indicate that in nature, when the kinetics of the reaction are taken into account, several reactions may occur simultaneously. As a consequence of this behavior, the observed mineral occurrences, if interpreted as equilibrium assemblages, will lead to the incorrect conclusion that the thermodynamic variance was lower than it actually was. This interpretation will also lead to incorrect calculations of the intensive variables, because the system is not as well determined as the interpretation suggests. This ambiguity between kinetic and thermodynamic models underscores the necessity to carry out careful textural analyses.

The instantaneous picture of disequilibrium, for either T or X_{CO_2}, over a reaction zone of the aureole at a particular point in time can also be plotted. Figure 14 is a plot of the instantaneous temperature profile in the reaction zone, for reaction 1, at $t = 1500$ yrs, with $\upsilon = 0.01$ *m/yr* and $k_1^0 = 4 \times 10^{-11}$ *moles/cm²/yr/(cal/mole)*. The vertical and horizontal lines

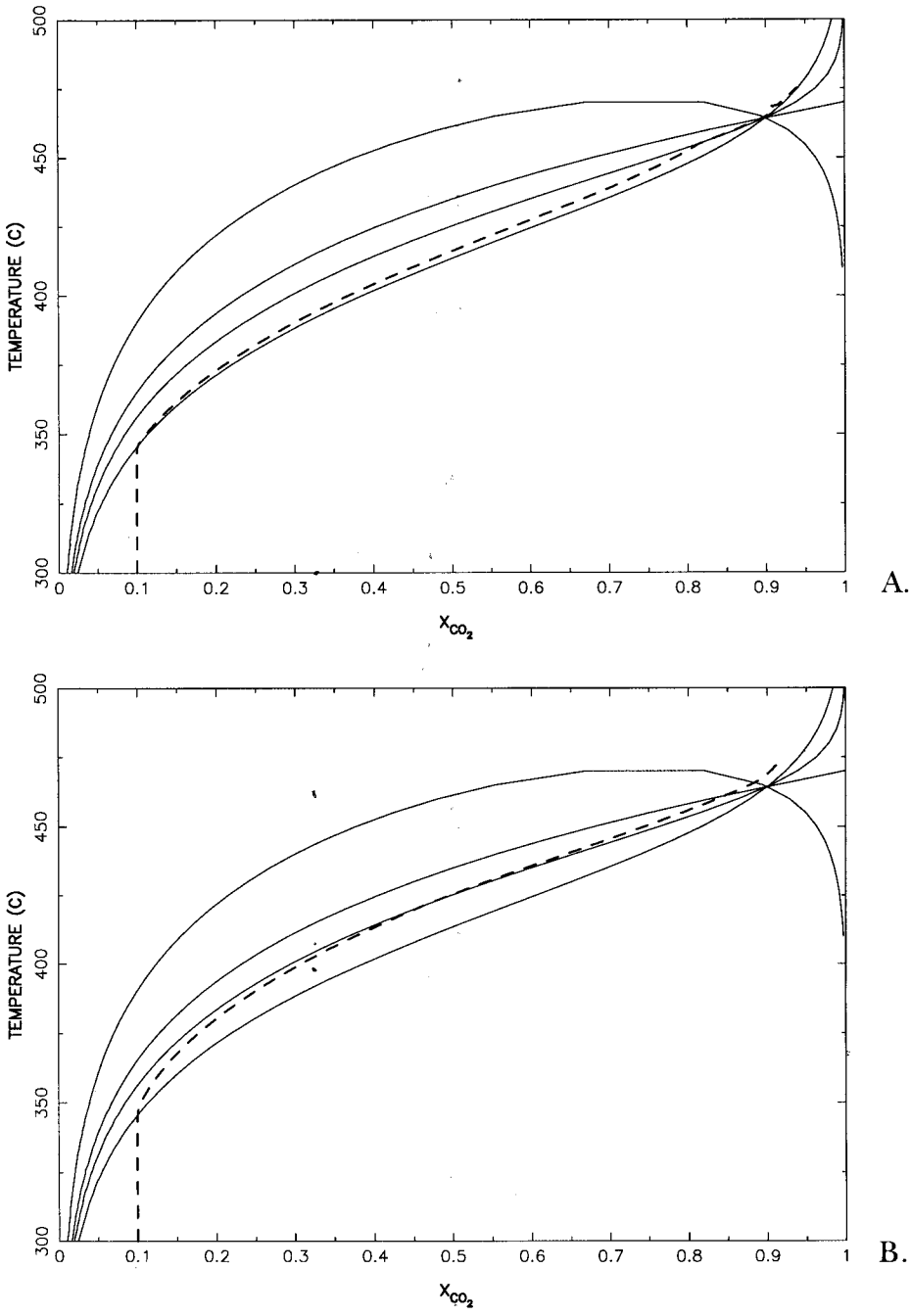

Fig. 12(A) T-X_{CO_2} evolution diagram for a rock sample 750 m from the contact and for the case $k_j^0 = 4 \times 10^{-9}$ $moles/cm^2/yr/(cal/mole)$ and for a fluid flow rate of $\upsilon = 0.01$ m/yr. The other variables are given in tables 4 and 5 and in figure 10. (B) T-X_{CO_2} evolution diagram for a rock sample 750 m from the contact and for the case $k_j^0 = 4 \times 10^{-10}$ $moles/cm^2/yr/(cal/mole)$ and for a fluid flow rate of $\upsilon = 0.01$ m/yr. The other variables are given in tables 4 and 5 and in figure 10.

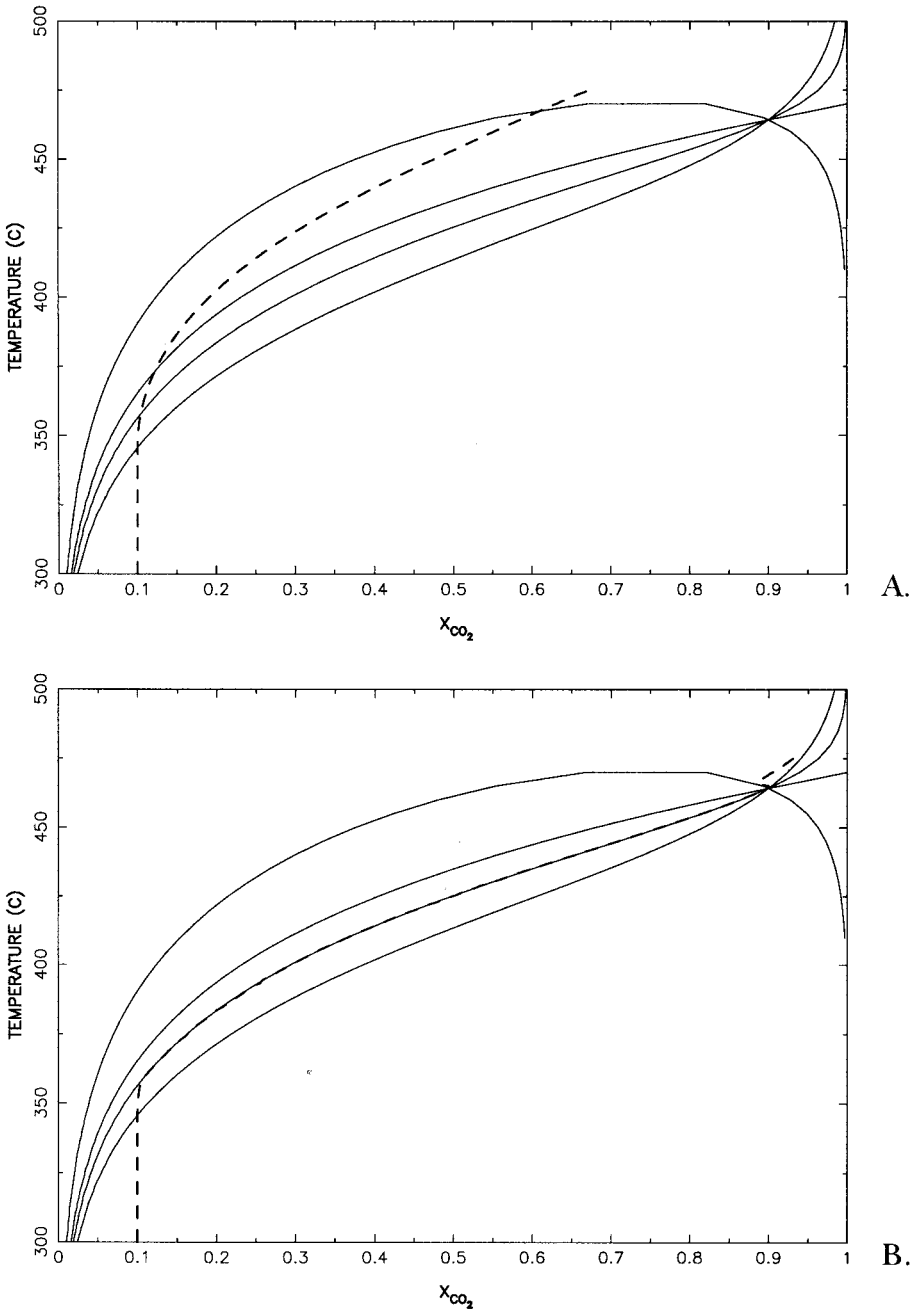

Fig. 13. T-X_{CO_2} evolution diagram for a rock sample 750 m from the contact and for the case $k_1^0 = 4 \times 10^{-11}$ $moles/cm^2/yr/(cal/mole)$ and for a fluid flow rate of $v = 0.01$ m/yr. The other variables are given in tables 4 and 5 and in figure 10. (A) The rates of reactions 2 and 3 were set to zero (that is they are independent on the tremolite surface area); (B) The rates of reactions 2 and 3 were set at a fast rate (k_2^0 and $k_3^0 = 4 \times 10^{-8}$ $moles/cm^2/yr/(cal/mole)$)

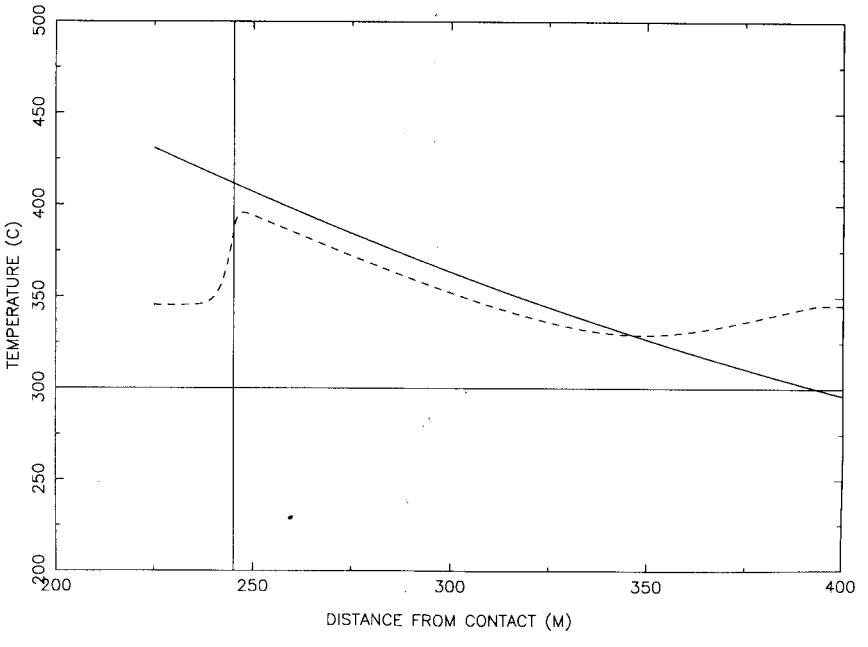

Fig. 14. Plot of instantaneous temperature profile in the reaction zone after 1500 *yrs*. $k_1^0 = 4 \times 10^{-11}$ *moles/cm²/yr/(cal/mole)* and $v = 0.01$ *m/yr*. The dashed curve indicates the equilibrium temperature corresponding to the fluid composition at the same location. Disequilibrium is indicated by the difference between the actual temperature (solid line) and the equilibrium temperature.

mark the boundary of the reaction zone and the 300°C reaction temperature cutoff respectively. The solid curve in the figure is the actual temperature profile as a function of distance from the contact. The dashed curve represents the temperature at which the fluid, with its particular local composition would be in equilibrium with reaction 1. Note that as the actual temperature drops below 300°C, this curve goes back toward the 348°C entry point, which is simply the T_{eq} for the initial X_{CO_2} of 0.01. However, there are two noticeable diffusion zones: one before the reaction zone, and the other near the cutoff zone (T < 300°C). The lack of equilibrium is seen throughout figure 14.

Figures 15, 16, and 17 show plots of the instantaneous X_{CO_2} fluid composition profiles in the reaction zone for different values of k_1^0 and v. The alternative plot for the conditions considered in figure 14 is shown in figure 15, where the actual X_{CO_2} composition of the fluid is plotted versus distance from the contact (solid curve). This curve is compared with the X_{CO_2} equilibrium curve (the X_{CO_2} values, which would lead to equilibrium of the fluid with reaction 1 at local temperatures). Again, there is a general disequilibrium, and there are two diffusion zones.

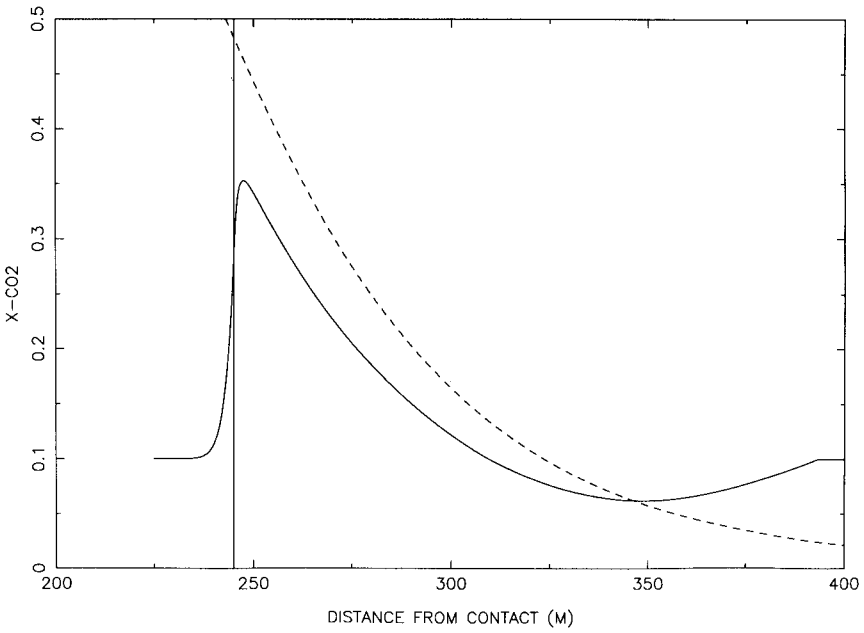

Fig. 15. Similar plot to figure 15 but now the instantaneous X_{CO_2} fluid composition is given (solid line). In this case, the dashed line is the value that X_{CO_2} would need to have for the fluid to be in equilibrium with the assemblage at the local temperature.

Figures 16 and 17 blow up the region near the reaction boundary for the case of faster kinetics, $k_1^0 = 4 \times 10^{-10}$ *moles/cm²/yr/(cal/mole)*. Figure 16 is for the case that $\upsilon = 0.01$ *m/yr*, whereas figure 17 is for the case $\upsilon = 0.1$ *m/yr*. Note that now the curves agree closely *away from the reaction boundary*. Using eq (51), the value of k_1^0 leads to a k_{eff} value of 0.085 yr^{-1}. For fluid flow rates of 0.01 *m/yr* and 0.1 *m/yr*, the values of $4Dk_{eff}/\upsilon^2$ are 0.07 and 1.1 respectively. Therefore, the fluid flow range where the transition from diffusion-dominated to flow-dominated process takes place is 0.01 to 0.1 *m/yr*. This prediction is verified nicely in figures 16 and 17. Figure 16 ($\upsilon = 0.01$ *m/yr*) shows diffusion dominating and extending outside the reaction zone. Meanwhile, figure 17 ($\upsilon = 0.1$ *m/yr*) shows the effect of fluid flow "shoving" itself inside the reaction zone for several meters, in agreement also with the simple kinetic model.

An even more profound result arising from the interaction of fluid flow with the rock will now be taken up. Early models assumed that *little* reaction took place along univariant lines and most of the reaction occurred at invariant points (Greenwood, 1975). This assumption was based on closed system arguments, small porosity, and fast kinetics. Other workers (Hewitt, 1973; Tracy and others 1983; Ferry and

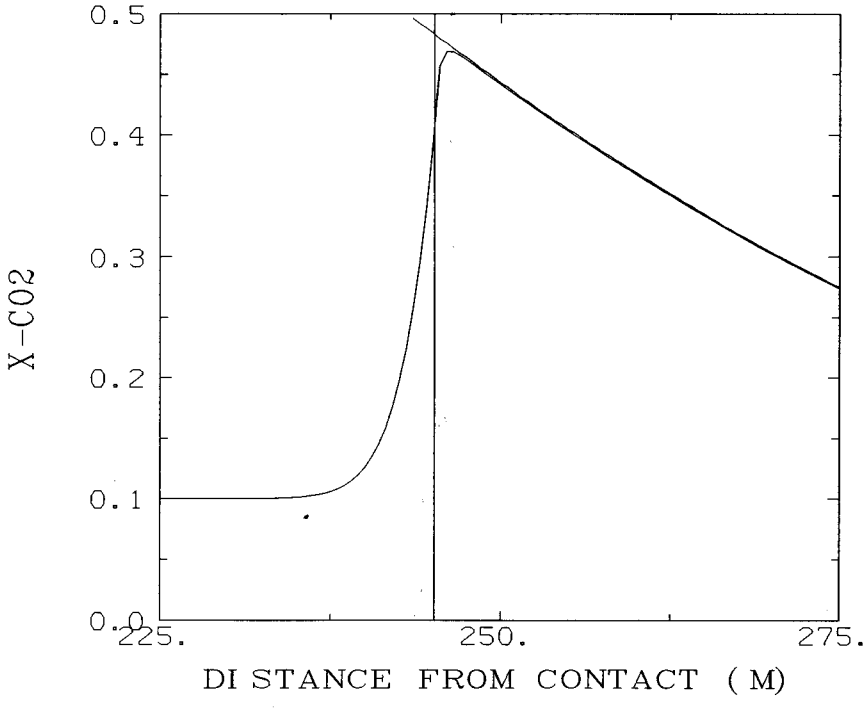

Fig. 16. Same as figure 15 but with $k_1^0 = 4 \times 10^{-10}$ *moles/cm²/yr/(cal/mole)*.

Baumgartner, 1991) have shown that significant reaction can take place in open systems. However their results were based on an assumption of local equilibrium, and their conclusions can be *severely* changed when reaction kinetics are taken into account. The basic problem can be outlined with the results of the simple kinetic model. Eqs (37) and (38) give the spatial region over which the fluid composition will *not* reach equilibrium. Note that if v is very small and k_{eff} is very large, then this distance is insignificant, and we regain the equilibrium assumption. Even for finite v, if the reaction rate is fast enough that eq (38) holds, then as k_{eff} keeps increasing, the non-equilibrium distance once more shrinks, and we also regain the usual assumption. However, if v is not zero and k_{eff} is not a very large number, then there will be a significant non-equilibrium region, given by either eq (37) or (38). Now if the fluid, even at steady state, has a non-equilibrium composition (for example, fig. 4), the solids will keep on reacting indefinitely until, depending on the size of k_{eff}, one of the reactants is consumed!

An illustration of the points made in the previous paragraph can be obtained within the metamorphic model outlined earlier and based on

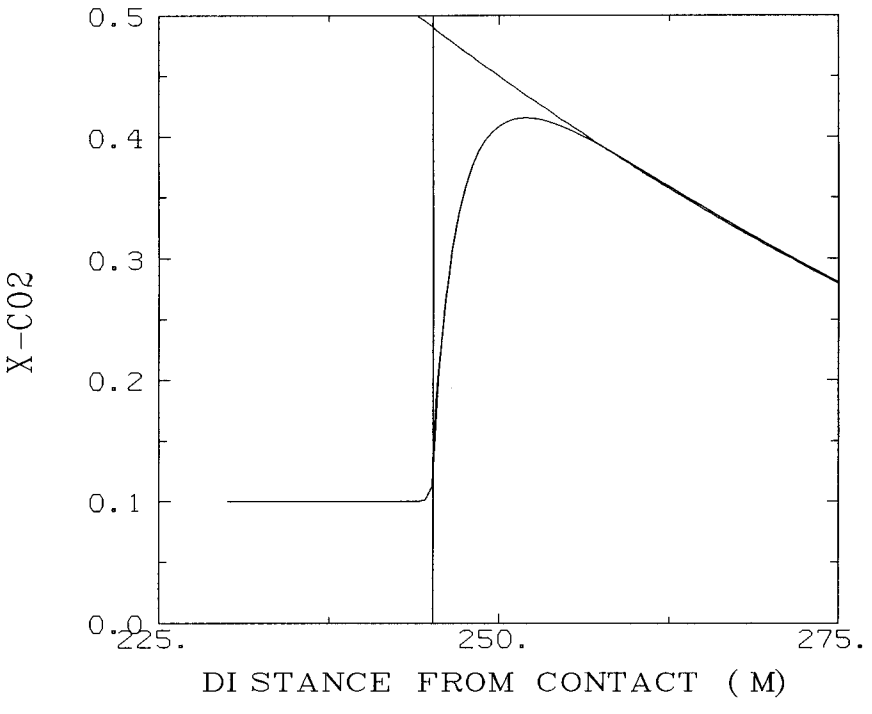

Fig. 17. Same as figure 15 but with $k_1^0 = 4 \times 10^{-10}$ *moles/cm²/yr/(cal/mole)* and $\upsilon = 0.1$ *m/yr.*

the reactions at the Marysville aureole. A calculation was made that allowed six of the reactions to take place (reactions 1, 2, 3, 4, 5, and 9 in table 2). The rate constants at 500°C for the six reactions were 4×10^{-10}, 4×10^{-10}, 4×10^{-8}, 4×10^{-10}, 4×10^{-8}, and 1×10^{-10} respectively (all in units of *mole/cm²/yr/(cal/mole)*). The activation energies of the six reactions were assumed to be 20, 20, 20, 20, 60, and 50 *kcal/mole* respectively. The rest of the parameters including the mineral abundances were the same as used in the earlier calculations in this section. The evolution of the temperature and fluid composition for a fixed position near the beginning of the reaction zone is shown by the dashed line in figure 18. Note that reactions 1 and 2 are both overstepped, and eventually the system has three metamorphic reactions operating **at the same time.** As the abundances of some of the reactant minerals decrease to zero, the fluid composition ceases to be buffered by the appropriate reactions, and the dashed line in figure 18 swings back to the water-rich initial composition. Therefore, the rocks in this locality never reach any of the invariant points. Nonetheless, the temporal sequence of mineral

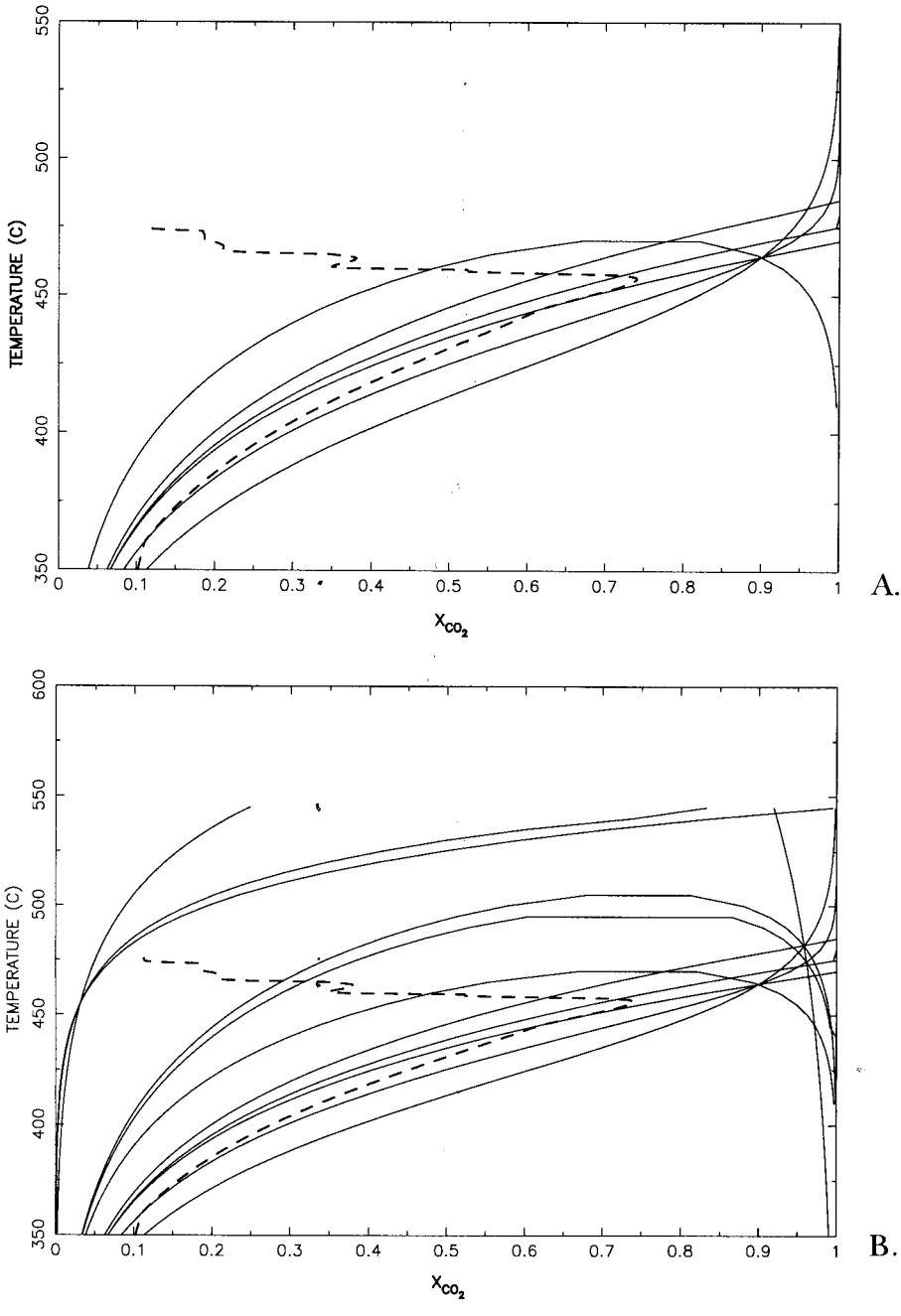

Fig. 18. T-X_{CO_2} path followed by the metamorphic fluid at a locality 1 m from the beginning of the reaction zone. (A) Dashed line shows the fluid composition path. Solid lines give the equilibrium T-X reaction curves for the 6 reactions used in the model. (B) Same as (A) but now all 12 equilibrium reaction curves (see table 2) are shown. Note the sharp change in fluid path as various different reactant minerals are consumed.

abundances mimics the spatial sequence in the field. Figure 19 gives the evolution of the mineral assemblage at the same locality. The abundances of the minerals are measured in this model by the radius of the mineral "spheres." Note that, in this particular calculation, the sequence in figure 19 corresponds to the sequence: Phlogopite-in, Tremolite-in, Phlogopite-out, Dolomite-out, Diopside-in. There is a minor resurgence of phlogopite at the end of the sequence because all the quartz is consumed before the dolomite is consumed. Lack of quartz shuts down reactions 2, 3, 4, and 5 and leaves the phlogopite producing reactions 1 and 9 operating.

It is important to stress that the details of the results in figures 18 and 19 will vary depending on variations in the initial conditions and the other parameters. No attempt is being made in this calculation to model accurately the details of the Marysville aureole (that is the topic of a forthcoming paper). Rather, the setting at Marysville is being used to point out some rather general conclusions. First, if the general conclusion of steady-state overstepping is acknowledged in cases involving fluid flow, then an important corollary that follows is the possibility of having several concurrent metastable metamorphic reactions taking place in the field. Such a scenario may be more common than is usually realized.

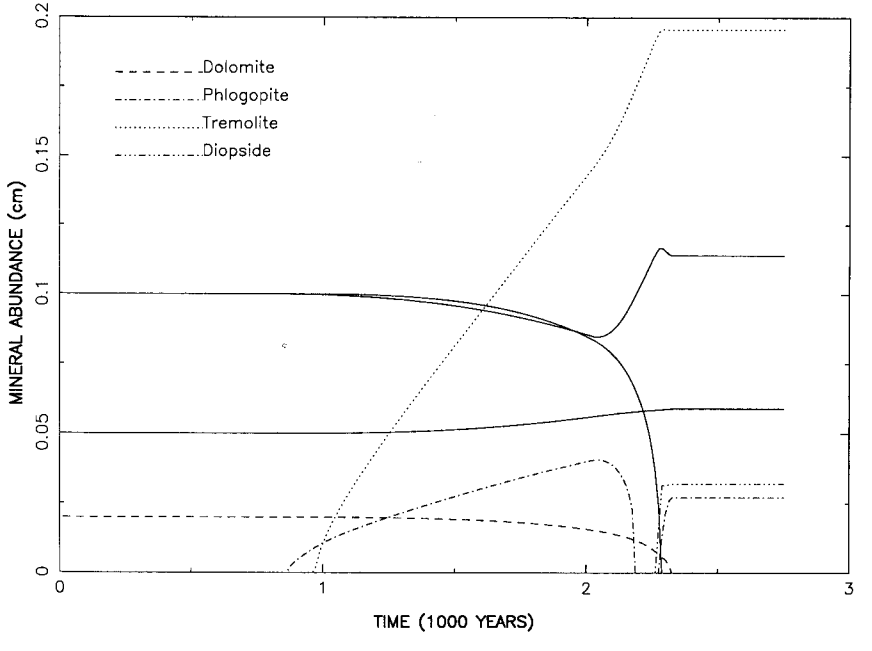

Fig. 19. Mineral abundances (reported as mineral radius in cm) as a function of time for the locality used in figure 18.

Second, the sequence of mineral assemblages produced in the kinetically controlled steady state region will be a function of initial mineral abundances just as in the case of a full equilibrium model. Third, the possibility of extensive reaction far from invariant points in open systems and the concurrent operation of several metastable reactions combine to produce a sequence of mineral assemblages that would in some instances be consistent with the sequence of reactions predicted by a full equilibrium model. Fourth, the fluid evolution in the non-equilibrium steady state region discussed at length throughout this paper may never reach the high CO_2 values expected at invariant points. Moreover, if such a scenario is followed, large amounts of "externally derived" fluids are allowed to interact with the rock, possibly explaining the large oxygen isotopic "shifts" observed at Marysville.

CONCLUSIONS

Several major conclusions can be drawn from this work. First and foremost, a critical concept that is needed to appraise properly the dynamics of systems that couple both fluid flow and the kinetics of chemical reactions is that of steady state. The establishment of steady state produces a region that is never close to equilibrium. The extent of this region for metamorphic systems was shown to reach lengths ranging from fractions of meters to at least hundreds of meters. Of great note is that these conclusions were reached using kinetic data measurable in laboratory time scales. At steady state, any locality not at equilibrium will remain so, until one of the reactant phases is completely consumed. As reactant phases are consumed, the region of non-equilibrium will shift in a manner governed by the details of the fluid flow, the thermal evolution, and the chemical kinetics within the reaction zone. Such steady state non-equilibrium regions can have a significant effect on our models of isograd development. For example, the equilibrium T–X_{CO_2} reaction curves may be significantly overstepped during metamorphic events. Furthermore, the overstepping of metamorphic reactions results in the possibility that several reactions can occur concurrently, including metastable reactions. In fact, this possibility requires us to keep track of all possible metastable reactions when considering observed phase assemblages. Extensive reaction far from invariant points in open systems and the concurrent operation of several metastable reactions will produce a sequence of mineral assemblages that, in some instances, would be consistent with the sequence of reactions predicted by an equilibrium model. This drastic deviation from the scenario based on no-flow and infinite-kinetics leads to the conclusion that isobaric invariant points and singular points may not necessarily be the loci of identifiable isograds in the field.

ACKNOWLEDGMENTS

Research was supported by the Branch of Energy Science of the Department of Energy (grant DE-FG02-90-ER14153), the Donors of the

Petroleum Research Fund, administered by the American Chemical Society (grant PRF 22364-AC2), and the U.S. National Science Foundation (grants EAR-9017976 and EAR-9105236).

We thank Jay Ague, Lukas Baumgartner, Mike Bickle, Jamie Connolly, Peter Lichtner, Roger Powell, Jack Rice, Alan Thompson, John Walther, and Bernie Wood for thoughtful and excellent reviews of various versions of the manuscript.

References

Ague, J. J., and Brimhall, G. H., 1989, Geochemical modeling of steady state fluid flow and chemical reaction during supergene enrichment of porphyry copper deposits: Economic Geology, v 84, p. 506–528.

Baumgartner, L. P. and Ferry, J. M., 1991, A model for coupled fluid-flow and mixed-volatile mineral reactions with applications to regional metamorphism: Contributions to Mineralogy and Petrology, v. 106, p. 273–285.

Bickle, M. J. and McKenzie, D., 1987, The transport of heat and matter by fluids during metamorphism: Contributions to Mineralogy and Petrology, v. 95, p. 384–392.

Brady, J. B., 1988, The role of volatiles in the thermal history of metamorphic terranes: Journal of Petrology, v. 29, p. 1187–1213.

Burnham, C. W., Holloway, J. R., and Davis, N. F., 1969, Thermodynamic Properties of Water to 1000°C and 10,000 bars: Geological Society of America Special Paper 132, 96 p.

Cathles, L. M., 1977, An analysis of the cooling of intrusives by ground-water convection which includes boiling: Economic Geology, v. 72, p. 804–826.

Chamberlain, C. Page, and Rumble, Douglas, III, 1988, Thermal anomalies in a regional metamorphic terrane: An isotopic study of the role of fluids: Journal of Petrology, v. 29, p. 1215–1232.

Connolly, J. A. D., and Thompson, A. B., 1989, Fluid and enthalpy production during regional metamorphism: Contributions to Mineralogy and Petrology, v. 102, p. 347–366.

Crawford, M. L., and Hollister, L. S., 1986, Metamorphic fluids: The evidence from fluid inclusions, *in* Walther, J. V., and Wood, B. J., editors, Fluid-Rock Interactions During Metamorphism: New York, Springer-Verlag, v. p. 1–35.

Dachs, E., and Metz, P., 1988, The mechanism of the reaction: 1tremolite + 3Calcite + 2quartz → 5diopside + $3CO_2$ + $1H_2O$: Results of powder experiments: Contributions to Mineralogy and Petrology, v. 100, p. 542–551.

Ferry, J. M., 1986, Reaction progress: A monitor of fluid-rock interaction during metamorphic and hydrothermal events, *in* Walther, J. V., and Wood, B. J., editors, Fluid-Rock Interactions during Metamorphism: New York, Springer-Verlag, v. p. 61–88.

———— 1987, Metamorphic hydrology at 13-km depth and 400-550°C: American Mineralogist, v. 72, p. 39–58.

———— 1991, Dehydration and decarbonation reactions as a record of fluid infiltration, *in* Kerrick, D. M., editor, Contact Metamorphism: Mineralogical Society of America, Reviews in Mineralogy, v. 26, p. 351–393.

Furlong, K. P., Hanson, R. B., and Bowers, J. R., 1991, Modelling thermal regimes, *n* Kerrick, D. M., editor, Contact Metamorphism: Mineralogical Society of America, Reviews in Mineralogy, v. 26, p. 437–505.

Greenwood, H. J., 1975, Buffering of pore fluids by metamorphic reactions: American Journal of Science, v. 275, p. 573–594.

Heinrich, W., Metz, P., and Bayh, W., 1986, Experimental investigation of the mechanism of the reaction: 1 tremolite + 11 dolomite = 8 forsterite + 13 calcite + 9 CO_2 + 1 H_2O: Contributions to Mineralogy and Petrology, v. 93, p. 215–221.

Heinrich, W., Metz, P., and Gottschalk, M., 1989, Experimental investigation of the kinetics of the reaction: 1 tremolite + 11 dolomite → 8 forsterite + 13 calcite + 9 CO_2 + 1 H_2O: Contributions to Mineralogy and Petrology, v. 102, p. 163–173.

Helgeson, H. C., and Lichtner, P. C., 1987, Fluid flow and mineral reactions at high temperatures and pressures: Journal of the Geological Society, London, v. 144, p. 313–326.

Hewitt, D. A., 1973, The metamorphism of micaceous limestones from south-central Connecticut: American Journal of Science, v. 273-A, p. 444–469.

Kerrick, D. M., and Jacobs, G. K., 1981, A modified Redlich-Kwong equation for H_2O, CO_2, and H_2O-CO_2 mixtures at elevated pressures and temperatures: American Journal of Science, v. 281, p. 737–767.

Korzhinski, D. S., 1959, Physicochemical Basis of the Analysis of the Paragenesis of Minerals: New York, Consultants Bureau Inc., 142 p.

Lasaga, A. C., 1981, Rate laws of chemical reactions, *in* Lasaga, A. C., and Kirkpatrick, R. J., editors, Kinetics of Geochemical Processes: Mineralogical Society of America, Reviews in Mineralogy, v. 8, p. 1–68.

———— 1984, Chemical kinetics of water-rock interactions: Journal of Geophysical Research, v. 89, p. 4009–4025.

———— 1986, Metamorphic reaction rate laws and development of isograds: Mineralogical Magazine, v. 50, p. 359–373.

———— 1989, Fluid flow and chemical reaction kinetics in metamorphic systems: A new simple model: Earth and Planetary Science Letters, v. 94, p. 417–424.

Lassey, K. R. and Blattner, Peter, 1988, Kinetically controlled oxygen isotope exchange between fluid and rock in one-dimensional advective flow: Geochimica et Cosmochimica Acta, v. 52, p. 2169–2175.

Lattanzi, P., Rye, D. M., and Rice, J. M., 1980, Behavior of ^{13}C and ^{18}O in carbonates during contact metamorphism at Marysville, Montana: Implications for isotope systematics in impure dolomitic limestones: American Journal of Science, v. 280, p. 890–906.

Lichtner, P. C., 1985, Continuum model for simultaneous chemical reactions and mass transport in hydrothermal systems: Geochimica et Cosmochimica Acta, v. 49, p. 779–800.

———— 1988, The quasi-stationary state approximation to coupled mass transport and fluid-rock interaction in a porous medium: Geochimica et Cosmochimica Acta, v. 51, p. 143–165.

Nagy, K. L., Blum, A. E., and Lasaga, A. C., 1991, Dissolution and precipitation kinetics of kaolinite at 80 C and pH 3: The dependence on solution saturation state: American Journal of Science, v. 291, p. 649–686.

Rice, J. M., 1977, Progressive metamorphism of impure dolomite limestone in the Marysville Aureole, Montana: American Journal of Science, v. 277, p. 1–24.

Rumble, D., III, Ferry, J. M., Hoering, T. C., and Boucot, A. J., 1982, Fluid flow during metamorphism at the Beaver Brook fossil locality, New Hampshire: American Journal of Science, v. 282, p. 886–919.

Schramke, J. A., Kerrick, D. M., and Lasaga, A. C., 1987, The reaction muscovite + quartz = andalusite + K-feldspar + water. Part I. growth kinetics and mechanism: American Journal of Science, v. 287, p. 517–559.

Skippen, George, 1974, An experimental model for low pressure metamorphism of siliceous dolomitic marble: American Journal of Science, v. 274, p. 487–509.

Steefel, C. I., and Lasaga, A. C., 1990, The evolution of dissolution patterns: permeability change due to coupled flow and reaction, *in* Melchior, D. C., and Bassett, R. L., editors, Chemical Modeling of Aqueous Systems II: American Chemical Society Symposium Series; v. 416, p. 212–225.

———— 1992, Putting transport into water-rock interaction models: Geology, v. 20, p. 680–684.

Thompson, J. B., Jr., 1959, Local equilibrium in metasomatic processes, *in* Abelson, P. H. editor, Researches in Geochemistry: New York, John Wiley, v. p. 427–457.

Tracy, R. J., Rye, D. M., Hewitt, D. A., and Schifferies, C. M., 1983, Petrologic and stable-isotopic studies of fluid-rock interactions, south-central Connecticut: 1. The role of infiltration in producing reaction assemblages in impure marbles: American Journal of Science, v. 283-A, p. 586–616.

Walther, J. V., and Wood, B. J., 1984, Rate and mechamism in prograde metamorphism: Contributions to Mineralogy and Petrology, v. 88, p. 246–259.

Wood, B. J., and Walther, J. V., 1983, Rates of hydrothermal reactions: Science, v. 222, p. 413–415.

———— 1986, Fluid flow and its implications for fluid-rock ratios, *in* Walther, J. V., and Wood, B. J., editors, Fluid-Rock Interactions During Metamorphism: Springer-Verlag, v. p. 89–108.

ERRATUM

FLUID FLOW AND CHEMICAL REACTION KINETICS IN METAMORPHIC SYSTEMS

ANTONIO C. LASAGA and DANNY M. RYE
Department of Geology and Geophysics, Yale University,
New Haven, Connecticut 06511

In this paper (May 1993, p. 361–404), please substitute eq 34 below for the one on page 373:

$$c'(x_r,t_r) = (c'_o - 1)e^{-(2-\alpha)x_r} + 1 + \frac{e^{-t_r}}{\sqrt{\pi t_r}} \int_0^\infty [c'(u,0) - (c'_o - 1)e^{-(2-\alpha)u} - 1]e^{-\alpha(u-x_r)} \cdot [e^{-(u-x_r)^2/t_r} - e^{-(u+x_r)^2/t_r}]du \quad (34)$$